CHARACTERIZATION OF VELOCITY AND SHEAR RATE DISTRIBUTION IN A CONTINUOUS MIXER

by

LINDSAY M. FANNING

A thesis submitted to the

Graduate School-New Brunswick

Rutgers, The State University of New Jersey

in partial fulfillment of the requirements

for the degree of

Master of Science

Graduate Program in Food Science

written under the direction of

Dr. J.L. Kokini

and approved by

_____

_____

_____

New Brunswick, New Jersey

May 2009

ABSTRACT OF THE THESIS

CHARACTERIZATION OF VELOCITY AND SHEAR RATE DISTRIBUTION IN A CONTINUOUS MIXER

By LINDSAY M. FANNING

Thesis Director:
Dr. Jozef Kokini

Computers simulations have been increasingly used to model mixing for uses in many industries. These simulations have given much insight into the mixing that takes place in different types of mixers. However, most computer simulations are unvalidated. Experiments have not been performed on the same systems to compare the results therefore the accuracy of a simulation is not precisely known. Validation is most important in complex systems or when working with fluids of a non-Newtonian nature. Understanding the mixing that takes place within the mixer allows for changes to be made to the mixer for different materials and aids in mixer design. In order to quantify the mixing taking place in a Readco two inch continuous processor, laser Doppler anemometry was used to measure fluid velocity. This velocity was compared to computer simulation results and was used to calculate the shear rate, length stretch, area stretch and mixing efficiency at different points within the mixer. With this information, the accuracy of the computer simulations was determined. Differences among the mixing of three fluids with different rheology were found. The mixing taking place in different areas of the mixer was assessed. Shear thinning fluids were found to be better mixed

with the paddle configuration used. The fluids were mixed best in the intermeshing region and between the tip of the paddle and the barrel wall.

Acknowledgement

- Dr. Jozef Kokini, my advisor, who gave me the opportunity and support to do this work and who had great patience for the time it took to complete.
- Dr. Robin Connelly, who has always been available with help and guidance for both the experiments and the writing, has provided much insight and advice, and has been an inspiring example of what is possible through dedication and hard work.
- Dr. Bharani Ashoken, who provided data from his computer simulations which made the completion of this work possible.

Dedication

This work is dedicated to my husband Brian who gave me the encouragement necessary to get it done and to my children, Owen, Patrick and Anna.

Table of Contents

Lists of Tables

List of Figures

Nomenclature

A	Area
A_v	Velocity gradient matrix
C	Cauchy-Green strain tensor
C_A	Concenctration fraction
C_f	Correction factor for fluid velocity
D	Stretching rate tensor
d_f	Fringe spacing
e_λ	Stretching efficiency
F	Deformation gradient
$G(\lambda,t)$	Length stretch probability function
$g(\lambda,t)$	Length stretch distribution function
$g_s(r)$	Eulerian concentration correlation
I_s	Intensity of segregation
k	Proportionality constant
L_s	Scale of segregation
$\bar{l}$	Length vector of the material
M	Local tangent unit vector
m	Present orientation vector
m_2	Refractive index of the fluid
N	Rotational speed of propeller
n_f	Refractive index
n_w	Refractive index of the cylinder wall

R	Radius
R_i	Inner radius of the cylinder wall
R_o	Outer radius of the cylinder wall
r	Radial position
r_a	Radius of beam intersection without refraction
r_f	True radius of the beam intersection position with refraction
t	Time
V,v	Velocity
$V\phi a$	Measured tangential velocity
$V\phi f$	Corrected tangential velocity
v_D	Doppler frequency
v_θ	Tangential velocity
X,x	Position of fluid element
y	Length vector of the material element
$\dot{y}$	Derivative vector
y'	Position of intersection without refraction
Δy	Change in position of the intersection point caused by refraction
α, α_1	Half angle between laser beams
$\bar{\bar{\Delta}}$	Shear rate tensor
γ	Shear strain
$\dot{\gamma}$	Shear rate
λ	Length stretch
λ_{MZ}	Manas-Zloczower mixing index

λ_w Wavelength of laser

κ Ratio of r to the outer radius

η Area stretch

Ω Vorticity

Ωi Angular velocity

I. Introduction

Mixing is one of the most common unit operations in the food industry. Consistent mixing is critical to food quality and reproducibility. Mixing traditionally has been a batch operation. With the need for increasing productivity in the food industry continuous mixers have become increasingly important. Because of their complex paddle geometry, continuous mixers are difficult to characterize. Small changes in the geometry and operation of the mixer can cause significant changes in its mixing characteristics and mixing efficiency. Mixing is not easily quantified analytically, numerically or experimentally. Quantifying parameters such as length of stretch and mixing efficiencies that measure distributive and dispersive mixing exist, but they are not able to be directly measured. Therefore it is hard to switch from established and conventional processes that work to those that may be better and more optimal but are not well defined.

Replacing batch mixers with continuous mixers has been slow in the food industry. This is largely due to the fact that the mixing in batch mixers is fairly well defined. Even though in common use, batch mixers have their disadvantages. Dead zones exist in them; which lead to longer mixing times or non-homogenous mixtures. Continuous mixers, on the other hand, are not quantitatively well understood and the extent of mixing is limited because the mixed material is subjected to mixing during a finite residence time. This lack of knowledge is due to the many configurations possible for a continuous mixer, all with their own mixing intensities. Each configuration would also have its own flow profile.

Before continuous mixers can effectively replace batch mixers in industry several questions need to be answered. The most important being how well does continuous

mixing compare to batch mixing? The geometrical setup of batch and continuous mixer differ a lot from one another. These differences are the cause of the extremely different flow patterns and mixing efficiencies. How the different flows in continuous mixing geometries affect the product outcome needs to be determined.

These ideas and knowledge base are the foundation of mixer design. The most promising way to develop design principles is to use computer simulation, because to experimentally evaluate the mixing efficiency of different mixers under different geometries and operating conditions would be very costly and time consuming.

However, computer simulation results need to be validated with accurate experimental results to make sure they reflect reality. Comparisons of calculated flow profiles and mixing efficiencies need to be made with an actual system in order to refine numerical simulation results. Unfortunately, experiments are somewhat limited by the nature of the material and unit operation. It is possible to test intermediate and finished products from an operation to determine their characteristics but this tells little about localized mixing in the mixer. Mixing can vary greatly from one region to another.

In order to better determine the mixing taking place within a mixer, a better local view needs to be taken. This work looks at the velocity distribution of fluid within a continuous mixer using laser Doppler anemometry (LDA). Using this technique, the velocity can be measured throughout the mixer. By measuring the velocity at each location, the mixing can be locally quantified. This quantification can lead to direct comparison between different locations within a mixer and with other types of mixers. LDA requires optical clarity so model fluids need to be used rather than actual food substances like doughs which are opaque. Using fluids of different rheology enables

comparison of the effect of fluid rheology on mixing efficiency. The knowledge gained from experimental measurements of mixing efficiency and the subsequent improvement in computer simulations of mixing will enable better mixer design.

II. Literature Review

A. Commercial Mixers

Mixers available to industry vary greatly in their design and setup depending on the operation they are being used for. Commercial mixers can be divided into two main groups; batch and continuous. They can be further divided based on their intended use. Different types of commercial mixers include agitated vessels, static mixers, dynamic mixers, extruders and homogenizers (Harnby, Edwards and Nienow, 1992).

Mixers can be classified according to the mixing mechanism they use. Blenders usually use a random distributive mixing mechanism and are able to be further divided based on the way they operate (Tadmor and Gogos, 2006). Tumbling mixers are the least expensive of the different types of mixers, however they have several drawbacks. Segregation can occur among the different components and an electrostatic charge can be produced while mixing powders. Ribbon blenders have some moving interior parts that produce some convective motion. They can be used to mix cohesive particulate mixtures. Cleaning is more cumbersome than for tumbling mixers and they too can generate static electricity. For low viscosity fluids, an impeller type mixer can be used. Sigma blade mixers can be used for fluids with a viscosity range of 0.5 to 500 N s/m^2 (Tadmor and Gogos, 2006). These mixers usually have small clearances so that stagnant regions do not form. There are also double blade mixers in which the blades overlap. For high viscosity liquids, mixers such as the Banbury can be used. These mixers provide laminar distributive mixing and provide dispersive mixing by having high shear stress areas that mixture components must repeatedly pass through.

Currently batch mixers are more commonly used in food processing than continuous mixer because of their perceived advantages. Continuous mixers are somewhat limited in the types of material they can mix because of the properties of the product and limitations on the amount of processing a product can undergo. Food products that are susceptible to over mixing are more difficult to mix in continuous mixers because the mixing is predetermined by the parameters set for the mixer. The amount of mixing achieved can not be changed once the process has been started. Batch mixers are better able to be adapted to different types of materials being mixed. The mixer can be stopped once the desired properties in the product are reached. There is no set amount of mixing time that the product must undergo. Batch mixers are easy to shut down for cleaning and can start without generating waste. Continuous mixers have difficulty being started and shut down which is needed for cleaning. It involves the waste of some material. Continuous mixers give better consistency in product quality than batch mixers, which can give some variation among batches.

Considerations that must be taken into account when choosing a mixer for a process include the vessel size and geometry needed for the desired process. The optimum choices are dependent on the properties of the material being mixed. The properties of the mixing impeller must also be taken into account. Impellers usually mix in either the radial or axial directions. Impeller choice depends upon the desired resulting mixing (Oldshue, 1983).

Agitated vessels are often composed of a vertical tank. They can include baffles to aid in the mixing. The mixing instrument inside the tank can be any number of paddles, propellers or turbines chosen to meet the needs of the mixing operation. Vertical spindle

mixers can be used for doughs. They are made up of several vertical spindles which hang down into a tub in which the material is mixed. The tubs are removable. They are suitable for many products and are particularly advantageous for types of dough that require a resting period since they can be removed for that time (Almond, 1988). Their main disadvantage is their speed and the physical work required to empty the tubs. They are slow so doughs requiring development time can take significantly more time than in other mixers. Ribbon mixers are often used for blending together ingredients. It is comprised of a u-shaped bowl and helical steel ribbons attached to a shaft that rotates. The ribbons are able to move the ingredients axially and radially providing adequate mixing. For high viscosity materials the tanks can be horizontal. Doughs that require development are usually mixed in high speed horizontal mixers (Matz, 1992). These mixers often use the roller bar type of agitator to mix since they can stretch and fold the dough without tearing it. A roller bar mixer is shown in Figure 1 along with a cross section showing the roller bars inside. The door on the mixer is on the lower half facilitating the removal of dough. Other types of mixing arms are also available for horizontal mixers. The arms used for hard doughs which require development usually contain both a round stretching portion and a scraping portion. The arms used for soft doughs are configured to mix as quickly as possible to avoid dough development (Almond, 1988). High speed mixers usually require short mixing times (Almond, 1988). The advantages of this type of mixer are their high throughput, the efficiency of some designs and the uniformity of the final product (Almond, 1988).

Figure 2 shows a single arm sigma mixer. Figure 3 shows a double arm sigma mixer and a cross section of its mixing blades. Double arm mixers are often used for lower

speed horizontal mixers when the dough does not require development such as for cookie or other sweet doughs (Matz, 1992). Static mixers consist of stationary mixing elements inside a pipe (Harnby, Edwards and Nienow, 1992). These elements mix the fluid as it flows through the pipe. The mixing increases with the number of elements. Dynamic mixers are used for emulsions, foams and finely dispersed solids (Harnby, Edwards and Niewnow, 1992). They are made up of a rotor spinning at high speed within a casing that is continuously pumped feed. Homogenizers are used to produce emulsions and dispersions. Extruders are also used in the food industry. They can be either single or twin screw. The feed is melted as it is pushed through the extruder at high pressure and out through a die at the end for shaping. Continuous mixers are usually used only on dedicated production lines because of the cost associated with them (Almond, 1988). They are often used to produce pasta and snack foods rather than doughs that are easily overworked (Almond, 1988). Figure 4 shows a continuous paddle mixer and what its paddles mixing elements inside look like. With a continuous mixer, material is constantly being supplied to the production line so there is not time for material to sit and change properties. The main disadvantage of using a continuous mixer is the problems with setting up the operation. They are not easily adaptable to dissimilar products and require expensive controls to feed and maintain everything going into the mixer (Almond, 1988).

Although continuous mixers do pose some challenges to their use in the food industry, their incorporation into product lines could improve the line. The mixing would be more efficient and work well for products that require higher shear. In order for this to happen, the mixing taking place in the continuous mixer needs to be better understood so

better design procedures could be developed. Better design procedures will lead to easier mixer placement in lines and consistant desired product quality.

Figure 1 Roller Bar Mixer and cross section http://www.shaffermanufacturing.com/mixing-systems/high-speed-roller-bar-mixers/supermixer-540-1000/default.html

Figure 2 Single Blade Sigma Mixer http://www.shaffermanufacturing.com/mixing-systems/single-sigma-mixers/supermixer-800-1600/default.html

Figure 3 Double Blade Sigma Mixer http://www.shaffermanufacturing.com/mixing-systems/double-sigma-mixers/supermixer-700-2300/default.html

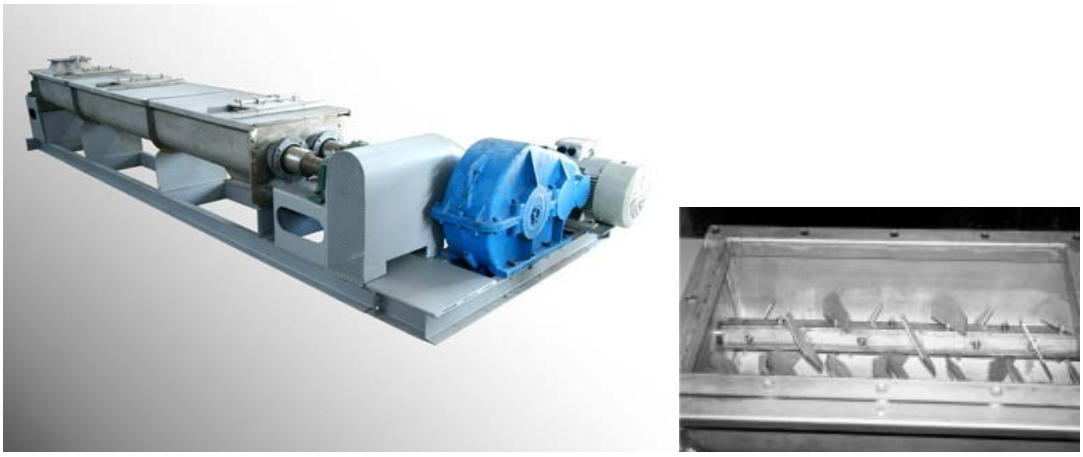

Figure 4 Paddle Mixer
http://www.ariaid.com/Web%20sites/AID/www.AID.com/ndk_website/AID/cmsdoc.nsf/webdoc/Paddle%20Mixer.html

B. Mixing

The purpose of mixing is to make a material homogenous. This takes place on two different scales. On a larger scale, a mixture can appear to be homogenous but on a molecular level it may still have agglomerations of solute. The two basic types of mixing are dispersive or intensive mixing and distributive or laminar or extensive mixing.

Dispersive mixing produces a size reduction of a component having a cohesive nature, while distributive mixing increases the interfacial area between components (Tadmor and Gogos, 2006). The goal of distributive mixing is to reduce the scale of segregation of the solute to a point where the material appears homogenous. Distributive mixing is mainly achieved in polymer processing through an increase in the interfacial area between the components of the system. This increase is a result of laminar shear, elongation, and squeezing deformation of the components (Tadmor and Gogos, 2006). On the molecular level, the material is mixed through diffusion. Diffusion is required to

obtain a truly homogenous mixture (Ulbrecht and Patterson, 1985). For very viscous materials, diffusion is very slow and does not provide much mixing to the mixture.

There are two different views that can be used to examine mixing; the Lagrangian or material and the Eulerian or spatial (Ottino, 1989). The Lagrangian view follows the motion of one fluid particle through the path it follows through the flow. The Eulerian view looks at what is happening to a fluid particle at a particular point and time.

1. Principles of Mixing

Mixing consists of the stretching and deformation of the material. The deformation of an infinitesimal filament is given by:

$$dx = F \cdot dX \qquad \text{Equation 1}$$

where F is the deformation gradient. This is shown in Figure 5. An infinitesimal point, a surface and a volume are deformed by the deformation gradient and the result is shown. A similar relationship exists for the deformation of a plane, which is given in Equation 2.

$$da = (\det F)(F^{-1})^T \cdot dA \qquad \text{Equation 2}$$

Strain can be measured by λ, length stretch, for an infinitesimal filament and η, area stretch, for an infinitesimal material plane.

$$\lambda \equiv \lim_{|dX|\to 0} \frac{|dx|}{|dX|}$$ Equation 3

$$\eta \equiv \lim_{|dA|\to 0} \frac{|da|}{|dA|}$$ Equation 4

When the deformation equation is substituted and M, the local tangent unit vector, is equal to dX/|dX|, the length stretch, Equation 3 becomes:

$$\lambda = \left(C : MM\right)^{1/2}$$ Equation 5

where $C = F^T \cdot F$ is the Cauchy-Green strain tensor. The specific rate of stretching of the length stretch is given by:

$$\frac{D(\ln \lambda)}{Dt} = D : mm$$ Equation 6

where *D* is the rate of stretch tensor and *m* is the present orientation. And the rate of change of the orientation of a material filament is given by:

$$\frac{Dm}{Dt} = m \cdot \nabla v - (D : mm)m$$ Equation 7

where *v* is the velocity. To create a measurement that is independent of the unit of time, the Cauchy-Schwarz inequality is used:

$$\frac{D \ln \lambda}{Dt} = D : mm \le |D||mm| = (D : D)^{1/2}$$ Equation 8

Therefore the stretching efficiency, e_λ, based on the length stretch is given by the equation:

$$e_\lambda = \left(\frac{D \ln \lambda}{Dt} \right) (D : D)^{1/2} \qquad \text{Equation 9}$$

The value of e_λ is -1 to 1. A value of -1 indicates unmixing. Based on their stretching efficiency, flows can be divided into three categories: flows that decay, flows with partial reorientation and flows with strong reorientation (Ottino, 1989). The behavior of these types of flow is shown in Figure 6. In Figure 6a flow with efficiency that decays is shown. After an initial jump in efficiency, there is a steep and steady decline in the efficiency which leads to an overall effect of little mixing having taken place. In Figure 6b flow with partial reorientation is shown. During the process, the efficiency has local peaks with some reorientation. In Figure 6c, flow with strong reorientation is shown. The process has a fluctuating reorientation but overall the mixture becomes more mixed.

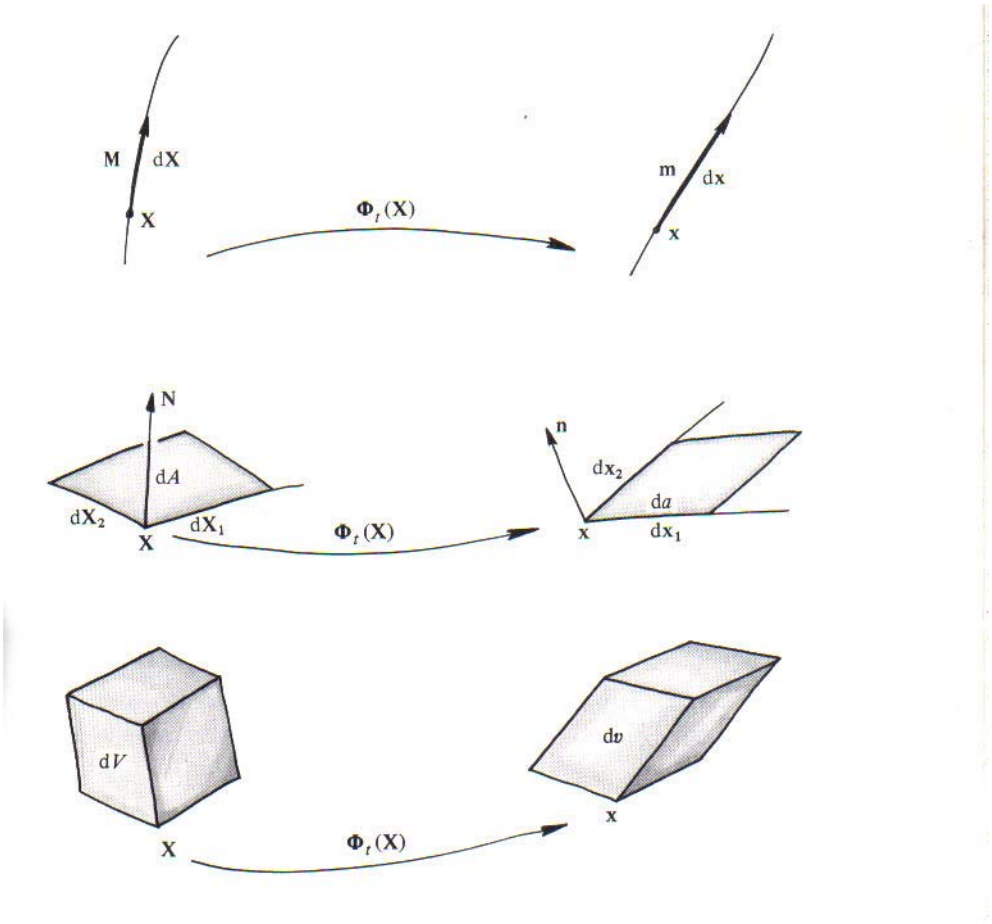

Figure 5 Deformation of infinitesimal elements, line surfaces, and volumes (Ottino, 1989)

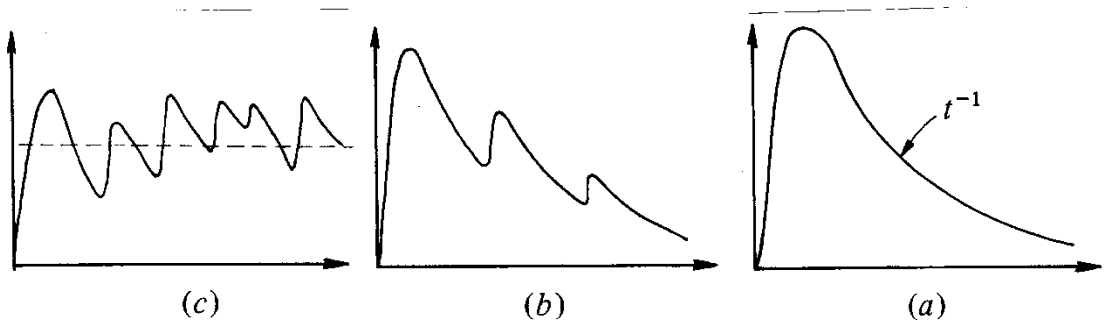

Figure 6 Typical behavior of mixing efficiency; (a) flow with decaying efficiency; (b) flow with partial restoration; and (c) flow with strong reorientation.

Through turbulent mixing, it is possible to reduce the size of agglomerates to a size at which they can only be separated more through molecular diffusion (Ulbrecht and Patterson, 1985). The scale of segregation, usually denoted as L_s, is the size scale of unmixed material. The value of L_s will go down as the material elements are stretched and divided in the mixing process. Another measure is the intensity of segregation, known as I_s, which is a measure of the concentration of neighboring fluid or material elements. The scale of segregation can be calculated using the equation

$$L_s = \int g_s(r)dr \qquad \text{Equation 10}$$

Where $g_s(r)$ is the Eulerian concentration correlation

$$g_s(r) = \frac{\overline{C'_A(x)C'_A(x+r)}}{\overline{C'_{A^2}}} \qquad \text{Equation 11}$$

In this equation $C'_A=C-C_A$ where C_A is the concentration fraction, r is the distance vector in space and x is the position in space. The intensity of segregation is defined by the equation

$$I_s = \frac{\overline{C_A'^2}}{\overline{C_{A0}}\left(1-\overline{C_{A0}}\right)} = -\frac{\overline{C_{A'}'C_B'}}{\overline{C_{A0}}\,\overline{C_{B0}}} = \frac{\overline{C_A'^2}}{C_{A0}'^2} \qquad \text{Equation 12}$$

This value is calculated from time averaged measurements at one point. In this form the segregation of two separate component streams being mixed is calculated. The value will range from zero to one with zero being complete mixing and one being complete segregation. (Ulbrect and Patterson, 1985) It is a measure of how the concentration changes.

The total strain that the components undergo is important to the final mixture characteristics because of its importance to laminar mixing (Tadmor and Gogos, 2006). The total strain that each fluid particle will experience depends on the type of mixer, operating conditions, and the fluid rheology. Strain distribution functions can be determined to help quantify the strain each fluid particle achieves. The function, $g(\gamma)d\gamma$ measures the fraction of fluid in the mixer that has undergone a shear strain from γ to $\gamma+d\gamma$. When the strain distribution function is integrated the following equation is obtained:

$$G(\gamma) = \int_0^{\gamma} g(\gamma) d\gamma \qquad \text{Equation 13}$$

where $G(\gamma)$ is the fraction of liquid in the mixer that has experienced a strain of less than γ. For a continuous mixer, the strain distribution function is defined as the fraction of fluid exiting the mixer that has experienced a strain between γ and $\gamma+d\gamma$ and is given by $f(\gamma)d\gamma$. Fluid particles in a continuous mixer experience different residence times and shear rates. When integrated, the strain distribution function gives the fraction of the exiting flow rate with strain less than or equal to γ, where γ_o is the minimum strain, and is given by the equation:

$$F(\gamma) = \int_{\gamma_0}^{\gamma} f(\gamma) d\gamma \qquad \text{Equation 14}$$

Both continuous and batch mixers have areas of high shear. For a continuous mixer these are small clearance places between the mixing paddles and wall of the mixer and between the two rotors for mixers with twin screws. In a batch mixer these regions are usually between the tips of the mixing blade and the mixer's wall.

2. Design Rules

Metzner and Otto (Metzner and Otto, 1957) studied the relationship between impeller speed and shear rate of the fluid in a baffled tank. The general relationship they developed was then used to interpret power consumption data from three non-Newtonian fluids. They presented an empirical design procedure based on their findings. The average shear rate of the system is first found using the equation:

$$\bar{\dot{\gamma}} = \left(\frac{du}{dr} \right)_{average} = kN$$

where k is a proportionality constant and N is the rotational speed of the propeller. The apparent viscosity is then determined from viscometric data using the calculated average shear rate. The Reynolds number could then be calculated and used to find the power number from their empirical data.

Earlier mixing studies have looked at differences in flow patterns in vessels using fluids of different rheological characteristics (Metzner and Taylor, 1960). Metzner and Taylor looked at flow patterns in an agitated baffled cylinder and compared those produced by Newtonian and non-Newtonian fluids. They found that local shear rates were directly proportional to impeller speed for both types of fluids, although they decreased more rapidly for pseudoplastic fluids with increasing distance from the impeller than with Newtonian fluids. The rate of power dissipation decreased as the

distance from the impeller increased. The velocity in the horizontal plane increased exponentially with impeller speed for the pseudoplastic fluid.

Metzner and coworkers extended this work to produce more far reaching design procedures (Metzner et al, 1961). In this work they quantified power requirements while changing tank diameter, impeller diameter ratio and type of impeller. They also further developed the prediction of power requirements for mixing pseudoplastics and Bingham plastics. They verified the direct proportionality between the average shear rate and impeller speed. They found proportionality constants for flat bladed turbines, fan turbines and marine propellers for purely viscous fluids. Power number – Reynolds number correlations were extended for these different types of mixers as well as for different impeller diameters. This allows for the same design procedure as outlined in previous work (Metzner and Otto, 1957) but gives empirical values for different types and sizes of mixers as well as for non-Newtonian fluids.

Another way to look at mixing is through examining the rate of mixing rather than the power consumption of the mixer. Norwood and Metzner (Norwood and Metzner, 1960) developed equations relating volumetric flow rates to the operating conditions of the mixer. They looked at mixing taking place in a baffled cylindrical vessel with a six bladed turbine.

More recent work has been done to expand and refine this work. Doraiswamy, Grenville and Etchells (1994) reviewed work done over forty years by researchers to examine the current state and usefulness of the Metzner-Otto correlation. They concluded that when working with close clearance impellers at low Reynolds numbers and with shear thinning fluids the correlation works for blend times as well as power

requirements and heat transfer. For turbines, the correlation does not work for mixing times because the shear rate is much lower than predicted. In transition and turbulent flows the correlation does not work that well because of higher shear rates around the impeller.

C. Mixing Efficiency

When determining how well mixed a mixture is, it can be looked at either quantitatively or qualitatively. Quantitative analysis gives a more thorough answer but is not always needed depending on the desired characteristics of the finished product. Qualitative comparison will often be sufficient when the compostion of the product does not affect quality. However, when it is important to the final outcome that the composition be the same in all samples, a more complete quantitative analysis is often required.

A quantitative measure of mixing will allow the evaluation of different processes to determine the most efficient one. Manas-Zloczower and Li (Chem Eng Comm, 1995) used length stretch, pairwise correlation function and volume fraction of islands as indexes to measure distributive mixing. In order to determine the mixing indexes, particles in the fluid must be able to be tracked, which can be done by knowing the velocity and flow fields through 3-D numerical simulation. By integrating the velocity vectors with respect to time the location of a particle can be found at any time by the following equation

$$\underline{X}(t) = \underline{X}(t_o) + \int_{t'=t_o}^{t'=t} \underline{v}(t')dt' \qquad \text{Equation 15}$$

where $\underline{X}$(t) is the location of the particle at any time t and $\underline{v}$(t) is corresponding velocity vector.

The length stretch is the rate of change of the distance between two particles and can be defined as

$$\lambda = \frac{\left|\underline{M}^{s}\underline{M}^{l}\right|}{\left|\underline{M}_{o}^{s}\underline{M}_{o}^{l}\right|} \qquad \text{Equation 16}$$

Where $\underline{M}^{s}_{o}$ and $\underline{M}^{l}_{o}$ are the initial locations of two particles and $\underline{M}^{s}$ and $\underline{M}^{l}$ are their locations at time t. It looks at the distance between the particles not the path they take. When Equation 3 and Equation 5 are used to calculate length stretch the motion of the particle is followed. If there are *I* clusters in a system with N_j particles in the *j*th cluster and only pairs consisting of particles from the same cluster are considered then:

$$\sum_{j=1}^{I} \frac{N_j\left(N_j - 1\right)}{2} \qquad \text{Equation 17}$$

is the total number of pairs in the system. The probability of having a pair with a certain length stretch is given by

$$G\left(\lambda,t\right) = \frac{M\left(\lambda,t\right)}{\sum_{j=1}^{I} N_j\left(N_j - 1\right)/2} \qquad \text{Equation 18}$$

where $M(\lambda,t)$ is the total number of pairs with length stretch ranging from $(\lambda-\Delta\lambda/2)$ to $(\lambda+\Delta\lambda/2)$ at time t. To present the results in term of the probability density function the relation

$$G(\lambda,t) = g(\lambda,t)\Delta\lambda \qquad \text{Equation 19}$$

is used where g(λ,t) is the length stretch distribution. The area under this curve is constant and does not depend on the distribution. The average value of λ at any time t can be found through

$$\overline{\lambda}(t) = \int_{\lambda=0}^{\lambda=\infty} \lambda g(\lambda,t) d\lambda \qquad \text{Equation 20}$$

The value obtained through Equation 20 quantifies how much the minor components of the same cluster of the mixture are spread away from each other. This can be used to evaluate a mixing process. The measure does not however, take into account regions in the mixer where none of the minor particles ever pass (Li and Manas-Zlocower, 1995 Chem Eng Comm).

Dispersive mixing is the breaking up of particles or droplets by reducing their length scale. Dispersive mixing efficiency can be quantified by taking into account elongational flow and the magnitude of stresses generated (Wang and Manas-Zloczower, 2001). Elongational flow can be quantified by comparing the magnitudes of the rate of deformation and the vorticity tensors in the equation

$$\lambda_{MZ} = \frac{|D|}{|D| + |\Omega|} \qquad \text{Equation 21}$$

λ_{MZ} ranges from values of 0 to 1, with 0 being pure rotation, 0.5 simple shear and a value of 1 pure elongation. For better dispersive mixing a value close to 1 would be desired.

Alemaskin, Manas-Zloczower and Kaufman (2004) developed a way to simultaneously measure the dispersive and distributive mixing taking place in a single screw extruder using the Shannon entropy. It is based on the probability of finding a particle in a specific volume of the space of interest. The best distributive mixing would take place when there are equal particle concentrations in each volume. They used a weighted average of the entropy for the different species in the system as a mixing index. When used with computer simulations and particle tracking to quantify the mixing using this new measure, it could be used for process design and optimization.

D. Laser Doppler Anemometry

Laser Doppler Anemometry (LDA) is used to measure fluid velocity. It is noninvasive and can be used for complex flows. Since LDA is an optical technique, it requires that the fluids and vessel be transparent. The system is comprised of a laser that is split and then sent into a Bragg cell. In the Bragg cell a frequency shift is created in one of the beams which allows for the direction of movement as well as the speed to be measured. The beams are transmitted into the test fluid at an angle to each other so they intersect within the fluid. The system measures light reflected by particles in the fluid as they pass through the measurement volume. The measurement volume is the point where the beams cross. The crossing of the beams creates interference which displays itself as light and dark regions called fringes. The space between the regions is called the fringe spacing. The frequency of the light that is reflected back is used to calculate the velocity of the particle and hence the velocity of the fluid.

The velocity is found through the following equations. First the half angle is found using Eqution 22 (Durst, 1981).

$$\sin(\alpha) = \frac{\lambda_w}{d_f \times 2} \qquad \text{Equation 22}$$

Where α is the half angle between the beams, λ_ω is the wavelength and d_f is the fringe spacing. The doppler frequency of the scattered light can be found using Equation 23 (Durst, 1981).

$$v_D = \frac{v}{d_f} \qquad \text{Equation 23}$$

where v_D is the Doppler frequency of the scattered light and v is the fluid velocity. Equation 22 and Equation 23can then be combined and solved for v to give the fluid velocity as shown in Equation 24.

$$v = \frac{v_D \lambda}{2 \sin \alpha} \qquad \text{Equation 24}$$

The two beams of the LDA system measure the velocity in different directions. Each set of split beams is projected into the barrel at 90° to the other set of beams and all cross at the same point. This allows for the determination of velocity in two directions with one measurement.

The main advantage of LDA is that it does not disturb the flow being measured. Measurements can be taken throughout the vessel and flow of interest. It is also possible to take measurements in all three directions at once. Because of the optical nature of LDA, there are certain limitations that arise. The fluid used and the vessel wall material must be optically clear to allow the lasers to pass through it unimpeded. Special equipment usually must be made to use LDA since most equipment does not have clear vessels. The vessel wall material can also cause refraction of the beams, so thick walls of

vessels cause difficulties in determining the point of beam intersection. Refraction must be taken into account when locating the position of the measurement volume. The fluid must be chosen with consideration to its optical properties which means that most real food materials can not be used because they are opaque. LDA has the capability to collect large volumes of data.

Prakash (Prakash, 1996) examined the mixing in a Brabender Farinograph using LDA. The Farinograph is a small scale batch mixer with small clearances between the blades and the wall. The velocity profile was found by taking measurements at 44 different locations within the bowl from perpendicular directions to measure three velocity components. Three model fluids were used: corn syrup, CMC and Carbopol. The shear rate, instantaneous area stretch efficiency, time averaged efficiency of mixing, strain rate, vorticity rate, dispersive mixing index, and lineal stretch ratio were calculated using the velocity profile. The average value of the lineal stretch ratio used to quantify distributive mixing was also found. With the data, Prakash was able to generate profiles for the calculated values within the mixer for each of the fluids used. She was able to show how shear rate varied for different parts of the mixer and how different rheology of each fluid affected the results.

Prakash (Prakash and Kokini, 1999) showed that mixing in the Brabender Farinograph was not homogenous. By examining the lineal stretch ratio, she revealed that the geometery of the mixer gave uneven mixing. More mixing was taking place between the two blades than between the blades and the wall.

Other work with LDA has been done by Bakalis (Bakalis, 1999) with an extruder. In his work, Bakalis found the velocity profile in the translational region for two screw

elements in a model co-rotating twin screw extruder. The two screw elements had different pitches. Diluted corn syrup and corn syrup mixed with 0.8% CMC were used. The velocity profiles were used to calculate the first invariant, the total shear rate, and a mixing index number. He found that the velocity components varied with the angular position and the depth at which the measurement was taken. It was found that the shear rate was not significantly different for the two types of screw elements.

Bakalis (Bakalis and Karwe, 2002) also found that there were higher velocities in the nip than in the translational section of the extruder. The measured volume flow rate was also higher in the nip region. The measured values agreed with calculated volumetric flow rate values.

Most work done using LDA to examine mixing has looked at the mixing in a stirred tank or the flow for other simpler systems. Lawler has looked at the flow of viscoelastic fluids through eccentric cylinders and a sudden axisymmetric contraction (Lawler et al., 1986). The behavior of fluids with different rheologies was studied. With LDA, the difference in behavior between the fluids was able to be seen. Schafer has used LDA to look at the flow caused by a rushton turbine in a stirred tank reactor (Schafer et al., 1997). The results were used to validate numerical simulation work. Schmidt et al examined the behavior of a low density polyethylene melt flowing through a slit die with a planar contraction of 14:1 (Schmidt et al, 1999). The measured velocity was used to obtain a viscosity function. This viscosity function was compared to viscosity functions obtained in other ways and showed the LDA measurements to be accurate. Fischer et al (Fischer et al, 2001) used LDA to measure the velocity near the wall of a channel. With this data it was determined how the Reynolds number affects the flow near the wall. Chen et al

(Chen et al, 1988) used LDA to relate the flow pattern in a baffled mixing tank to the impeller type. The flow in the tank was also further characterized in order to help improve modeling. Mavros et al (Mavros et al, 1997) used LDA to look at a Rushton turbine and axial flow Mixel TT agitator with a stream of liquid entering to examine the effect on the flow.

E. Optical Experimental Techniques

Other optical techniques exist that have different advantages and disadvantages from laser Doppler anemometry. Some of these techniques fall under the broad category of pulsed light velocimetry (PLV) in which particle markers are recorded as images two or more times (Adrian, 1991). PLV can be further broken down into photochromic and fluorescent which track molecular markers and high image density PIV and low image density PIV.

Particle image velocimetry (PIV) is an experimental method in which particles in a flow are tracked using a pulsed sheet of light produced by a laser. Images are taken at 90˚ to the sheet and then analyzed to determine the velocity magnitude and direction of the fluid flow for small areas of the cross section (Adrian, 1991). PIV can be broken down into low image density mode and high image density mode. In low image density mode, the number of particles in the fluid is low enough that individual particles can be tracked in the recorded images. Low image density mode PIV is also referred to as particle tracking velocimetry (PTV). In high image density PIV there are more particles in the flow than PTV but not enough that the particles overlap. The displacement of small groups is normally measured in this type of PIV, since tracking the individual particles would be much more time consuming (Adrian, 1991). Unlike LDA these

techniques are not able to measure velocity in all three directions at the same time since only particles in the lighted plane are measured. PIV allows for the following of one particle through the fluid if flow is 2-D and within the lighted plane. Computer analysis of the recorded images can be very time consuming depending on the number of particles in the interrogation spot. Actual measurements can be made more quickly than with LDA because an entire plane is measured at once compared to individual point measurements. Measurements are accurate throughout the field but less so in regions where the velocity is rapidly changing (Adrian, 1991).

Unger, Muzzio, Aunins and Singhvi (2000) used PIV to study the mixing in a roller bottle bioreactor. They used their experimental results to validate results from a computational fluid dynamics simulation. They found that their experimental results correlated well with their simulation results. PIV was also used by Arratia, Kukura, Lacombe and Muzzio (2006) to examine the mixing of shear thinning fluids with yield stress in a stirred tank. With PIV they were able to obtain velocity profiles for a planes with in the vessel. Along with PIV, planar laser induced fluorescence (pLIF) was used for flow visualization. Like PIV, pLIF uses a laser sheet passed through the fluid. An image is recorded with a camera of a tracer distribution within the fluid. CFD simulations were also performed, and the results were compared with the experimental results through the root mean square deviation. They found that in their range of Reynolds numbers, chaotic dynamics controlled the mixing of the shear-thinning yield stress fluid.

F. Computer Simulation of Mixing

Connelly and Kokini (2004) have used FEM flow profiles of a simplified mixer to compare the effects of fluids with different rheological properties. Newtonian, inelastic Bird-Carreau and Oldroyd-B models were first used and the Phan-Thien Tanner model which takes into account both viscoelasticity and shear thinning. The differences for the velocity profile among the models were only slight, but when mixing indices were used to measure the mixing the differences were obvious. Several different measures of mixing were used for the comparison. Scale of segregation, cluster distribution index, the natural log of the length of stretch, and mean length of stretch were all calculated. Using these results along with particle tracking, the effectiveness of the mixer was able to be determined.

Connelly and Kokini expanded their work (2007) to include simulations of a twin screw co-rotating mixer. They again used FEM simulations to produce flow profiles and to track particles. Comparisons were made between a model single screw mixer and a twin screw mixer modeled after the Readco continuous processor. Segregation scale, the cluster distribution index, the length of stretch and the mixing efficiency were calculated. They determined that dispersive mixing was highest in the intermeshing region of the twin screw mixer. Regions of plug flow exist in both mixers, which results in little mixing in these areas. The simulations show that despite the large plug flow areas, the twin screw mixer is more effective than the single screw mixer.

III. Materials and Methods

A. Materials

1. Description of the Continuous Mixer

The continuous mixer used for this work was the 2 inch, twin screw, Continuous Processor (Readco, York PA). It is a twin screw mixer with rearrangable mixing elements. The mixing elements on the two shafts are oriented at 180˚ to each other. The barrel is 18 inches long. Each shaft of the barrel is 2 inches in diameter with an intermeshing region. The material enters the mixer by passing through a hopper. Intermeshing co-rotating feed screws draw the material into the mixer. The mixer is then fitted with either flat or helical paddles in four possible positions. At the end of the two shafts is a reverse helical paddle that directs the fluid out of the mixer. The screws rotate at the same speed, which was measured by a tachometer. A Plexiglas barrel was fabricated to allow the inside of the barrel to be viewed during operation and to make it transparent to lasers and other optical techniques. The mixer has an end plate with an adjustable opening that can be opened or closed to slow the flow coming out of the mixer. The mixer is shown in Figure 7.

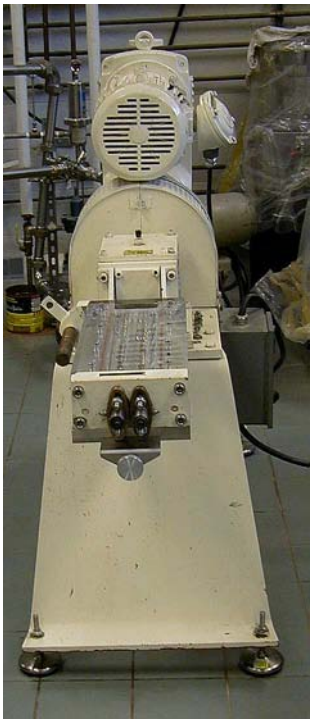

Front View

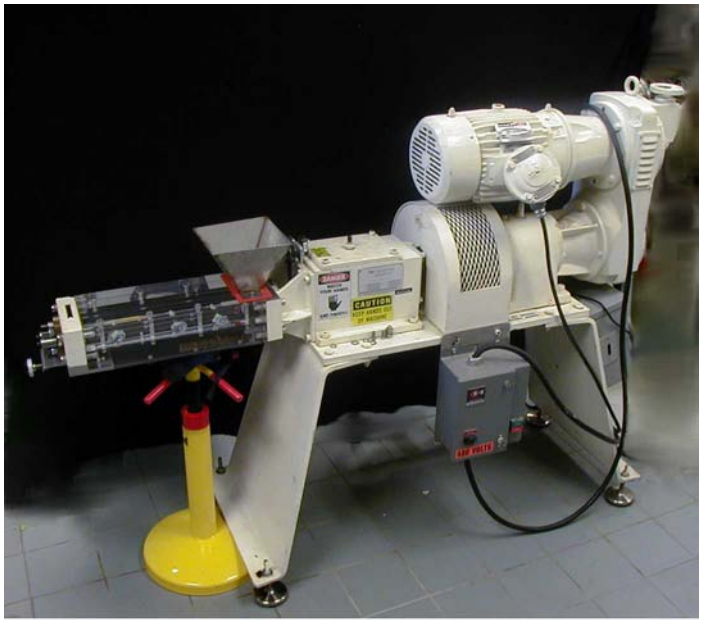

Side View

Figure 7 : Readco Continuous Processor

2. Laser Doppler Anemometry

A two color, Argon ion laser Doppler anemometer (Dantec Dynamics, Mahwah NJ) was used to measure local fluid velocities. A schematic diagram of the system setup is shown in Figure 8. A laser is generated and sent into the Bragg cell where it is split and a frequency shift is created in one of the beams. The frequency shift allows for the measurement of the direction as well as the magnitude of the velocity. The beams are emitted from a probe into the fluid whose velocity is being measured. There are two beams of the same color for each direction being measured. To measure multiple velocity components at once, a set of beams is needed for each component. The planes that these sets of beams are in are perpendicular to each other. All of the beams are sent in at an angle to their corresponding beam of the same color and cross at one point. This point is where the measurement is taken. The crossing of the beams creates a measurement volume made up of interference fringes which displays itself as light and dark regions. These regions have a particular spacing, called the fringe spacing, between them that depends on the angle between the beams. Particles in the fluid that pass through the measurement volume scatter light from the beams. The frequency of the scattered light is measured by the probe and then converted to velocity using Equation 24.

The only parameter measured in this equation is the frequency of scattered light (v_D), all the other variables are determined by the settings of the LDA system. The probe is on a 3-D traverse that allows for accurate positioning to 0.1mm.

An encoder was connected to measure the rotation of the mixer shafts accurately. The encoder was able to measure 360 times every rotation so it marked every degree of

rotation to ±3˚ accuracy. The LDA was set up to take measurements from the top of the clear barrel of the mixer. The settings used for the LDA are shown in Table 1.

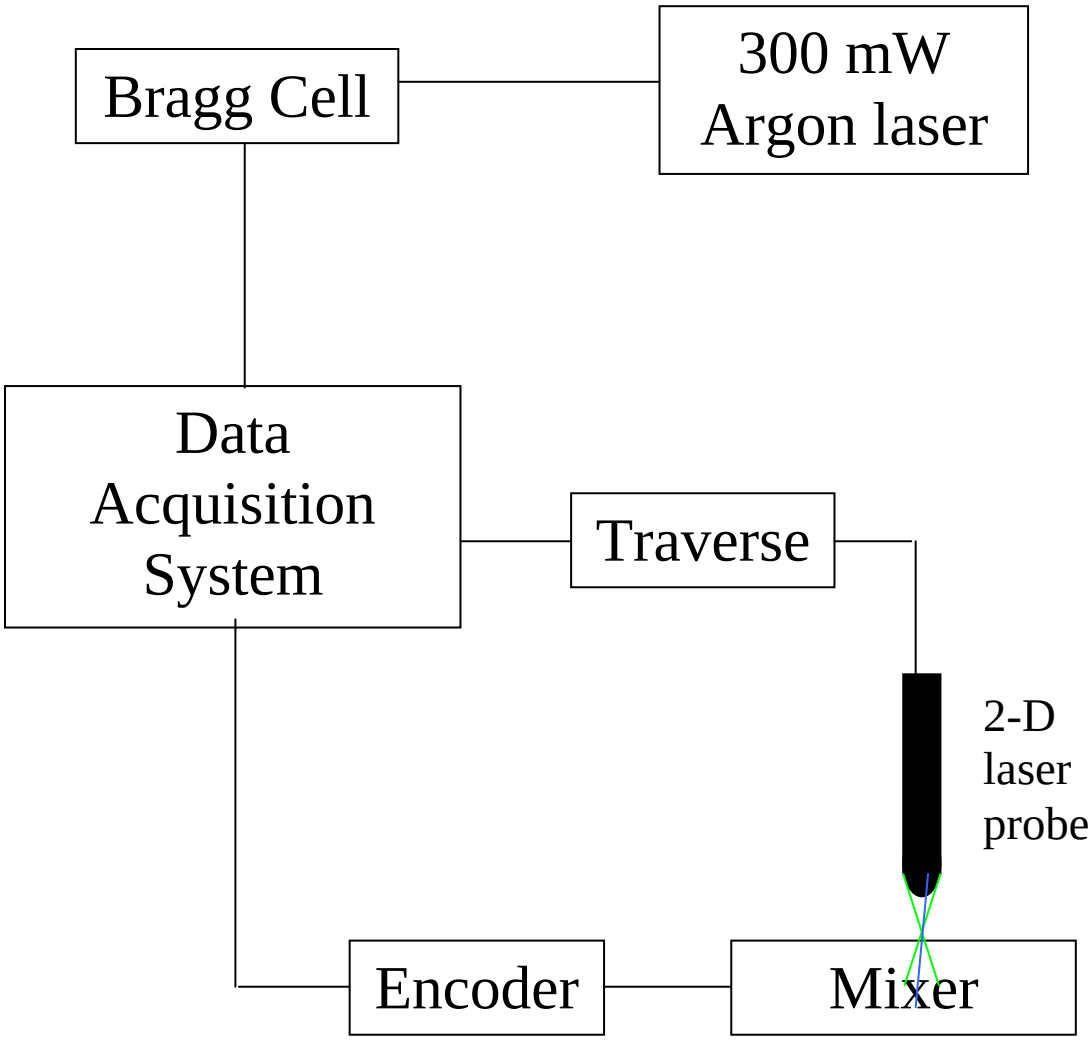

Figure 8 Schematic of LDA system

LDA Settings	
Probe Lens Focal Length (mm)	120
Bragg Cell Frequency Shift (MHz)	40

	Blue Beam	**Green Beam**
Wavelength, λ (nm)	488	514.5
Number of Fringes	60	60
Fringe Spacing (μm)	1.5602	1.6449

Table 1 Settings used for LDA system

3. Model Fluids

Three fluids were selected for these experiments to model different rheological behaviors: corn syrup, carboxymethyl cellulose and Carbopol. These fluids were previously used in mixing studies by Prakash (Prakash, 1996) to represent Newtonian and increasingly shear thinning rheology.

Globe corn syrup 1142 (Corn Products International) was used as the Newtonian fluid. This corn syrup is a regular conversion, ion exchanged syrup with a dextrose equivalent of 42.0 D.E. This syrup has a viscosity of 74,000 cps at 80˚F.

A 2% solution of sodium carboxymethyl cellulose (CMC) type 7HOF (Hurcules Inc.) was used as a non-Newtonian fluid. CMC is a cellulose ether and a long chain polymer with a molecular weight of 700,000. The molecular weight is determined by the degree of polymerization and the degree of substitution. The greater the molecular weight the

higher the viscosity. Viscosity is also dependent on how neutralized the carboxymethyl groups are. Type 7HOF has a degree of substitution of 0.7, high viscosity and is food grade. It has some pseudoplastic behavior (Hercules Inc, 2000). It was prepared by slowly adding the powder in a vortex of water produced by a propeller mixer and then allowed to mix for fifteen minutes. The solution was then allowed to stand overnight so air bubbles could come out of the solution.

A 0.011% dispersion of Carbopol 940 (Noveon) was used to represent the behavior of Xanthan gum. A 0.011% dispersion of Carbopol 940 and a 0.5% solution of Xanthan gum have similar properties but Carbopol has better clarity so is better suited for these experiements (Prakash, Karwe and Kokini, 1999). Carbopol is an acrylic acid polymer. To attain the maximum viscosity from a Carbopol dispersion, it must be neutralized so the polymer will uncoil and be able to fully hydrate. The carbopol was prepared by adding to a vortex of deionized water that was produced from a propeller type mixer and then adding a 10% solution of sodium hydroxide to neutralize the dispersion. The dispersion was mixed for an additional fifteen minutes. The carbopol was then allowed to sit overnight to allow the molecules to become completely dispersed.

Rheological measurements were performed with the Advanced Rheometric Expansion System (ARES) (Rheometric Scientific, Inc., Piscataway, NJ). Results are shown in Figure 9 and Figure 10 for CMC and carbopol respectively. Measurements were preformed in triplicate and then averaged together to produce the shown results.

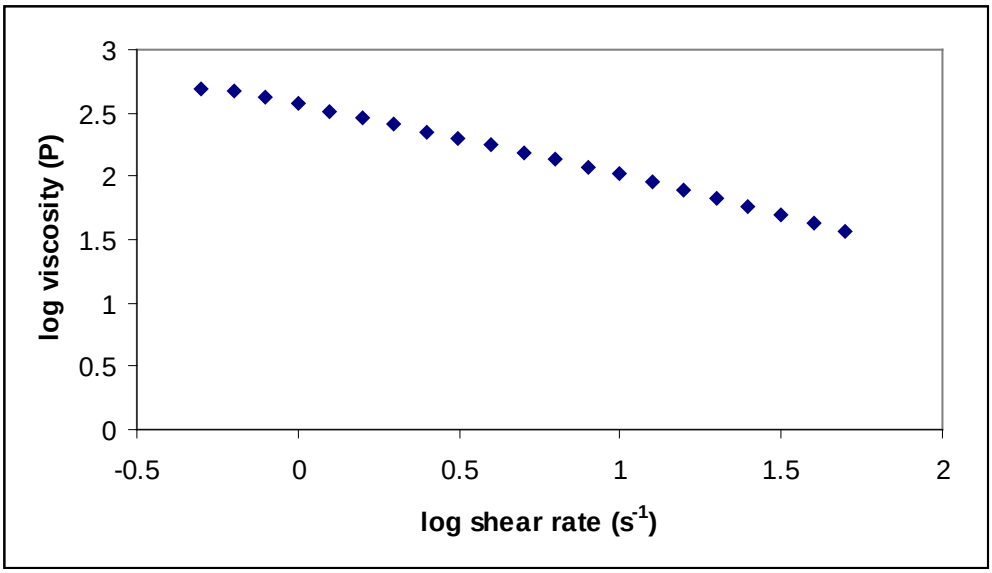

Figure 9 Variation of viscosity with shear rate for CMC

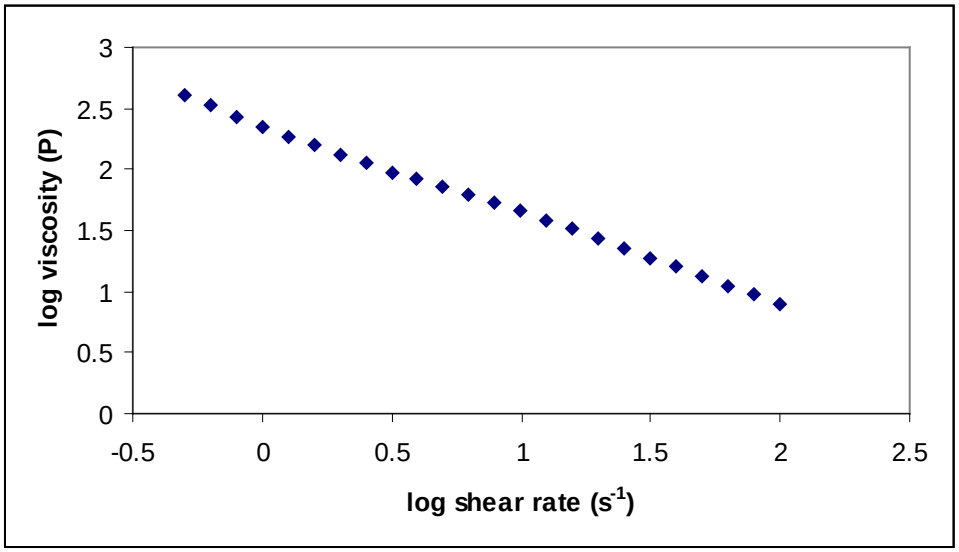

Figure 10 Variation of viscosity with shear rate for Carbopol

B. Methods

The experiments conducted focused on the following objectives:

- Verify the accuracy of the LDA by measuring velocities in a well defined couette flow system where the accurate velocity distribution is available analytically.
- 2. Measure the velocity distribution of each of the three fluids in a Readco Continuous Processor.
- 3. Calculate local shear rate distribution and mixing indices from the measured velocity distributions.

1. Experimental Couette Setup for Verification of LDA Measurements

The accuracy of the LDA measurements was determined by first using the LDA to measure the velocity of couette flow in a Couette device. Since the analytical solution for the velocity of couette flow is well known, the measured velocity can be easily compared with the calculated value. For this purpose a transparent couette system was constructed.

The inner cylinder had a diameter of 69 mm. The diameter of the outer cylinder was 104 mm. The space between the cylinders was filled with corn syrup. The inner cylinder rotated at 20 rpm. The speed of the inner cylinder was set using a hand held tachometer. The LDA and couette were set up as shown in Figure 11. The LDA measurements were taken along the center line of both cylinders with the beams oriented so they measured the tangential and axial velocity. The axial velocity should be 0 m/s in couette flow if secondary flows are negligible. Secondary flows are negligible for relatively low angular velocities where inertial effects and centrifugal forces are negligible. The angular velocity which is only a function of the radial position *r*, was calculated using (Bird, 2002):

$$v_\theta = \Omega_i \kappa R \frac{\left(\frac{R}{r} - \frac{r}{R}\right)}{\left(\frac{1}{\kappa} - \kappa\right)} \qquad \text{Equation 25}$$

where $\mathbf{v_\theta}$ is the tangential velocity, $\mathbf{\Omega_i}$ is the angular velocity, **R** is the outer radius, **r** is the radial position and $\boldsymbol{\kappa}$ is the ratio of r to the outer radius.

Velocity was measured at 5 different points on the radius. The measurements taken at each point were averaged and corrected for the refraction caused by the curvature of the outer cylinder and corn syrup. The correction factor was calculated with Equation 26 (Bicen). To find the actual intersection point of the beams, the calculated correction factor is then used in Equation 27. To calculate the corrected velocity Equation 28 was used.

$$C_f = \frac{1}{n_f}\left[1 + \left(\frac{r_a}{R_o}\right)\left[\left(\frac{R_o}{R_i}\right)\frac{\left(\frac{n_f}{n_w} - 1\right)}{n_f} + \frac{n_w - 1}{n_w}\right]\right]^{-1} \qquad \text{Equation 26}$$

$$r_f = C_f r_a \qquad \text{Equation 27}$$

$$V_{\phi f} = C_f V_{\phi a} \qquad \text{Equation 28}$$

C_f is the correction factor for fluid velocity, n_f is the refractive index of the fluid, r_a is the radius of beam intersection without refraction, R_o is the outer radius of the cylinder wall, R_i is the inner radius of the cylinder wall and n_w is the refractive index of the cylinder wall. The true radius of the beam intersection position with refraction is r_f, $V_{\phi f}$ is the corrected tangential velocity and $V_{\phi a}$ is the measured tangential velocity.

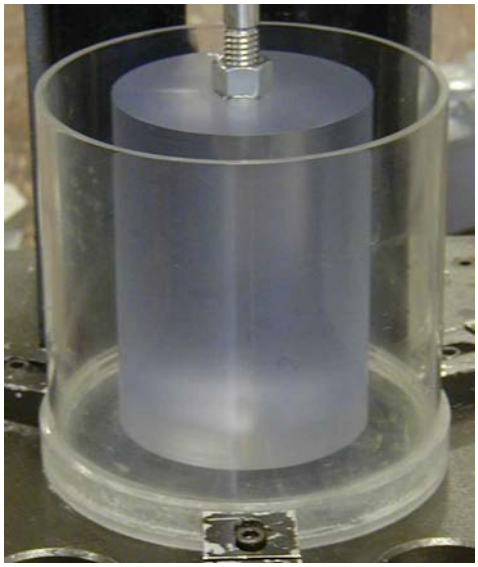

a) Couette cup and bob

b) Couette measurement set up

Figure 11 Set up for Couette Measurements

2. Measurement of Velocity in the Continuous Mixer

Velocity was measured in the Readco Continuous Processor using Laser Doppler Anemometry. A Plexiglas barrel which was an exact replica of the original stainless steel barrel was constructed for the mixer so the laser beams would be able to pass through the barrel and enter the fluid. The mixer was configured, starting at the inlet, with two feed screws, nine flat paddles all aligned, another feed screw and then one reverse helical paddle. Measurements were taken on five different cross sections; the first flat paddle, the fourth flat paddle, the seventh flat paddle, between the ninth flat paddle and the feed screw following it, and 30 mm into the third feed screw. The measurement planes are shown in Figure 12. The shaft orientation was measured by an encoder which was connected to one of the shafts. The starting 0˚ position is shown in Figure 13 along with the coordinate system.

Forty points were measured in each cross section. The points measured are shown in Figure 14. Data was taken at the forty points for each of the five cross sections. The traverse was programmed to move to each point sequentially. In order to calculate the velocity gradient, the traverse also moved the probe to take measurements 2mm away from the original point in the x, y and z directions. The velocity measured at each point was sorted by the encoder position and then averaged. The position of each point was corrected due the refraction caused by the beams passing through the barrel.
Because of the fluid, the curvature of the inside of the barrel and the thickness of the barrel, refraction needs to be taken into account when determining the position of the measurement volume is located. The beams entering the barrel will be bent to a different angle and will meet at a different location. Because of the similarity of the refractive

indexes of the Plexiglas and the fluids, the barrel and fluid can be treated as a solid block and the curvature can be neglected. This greatly simplifies the refraction calculation required to locate the measurement volume's location. The new location can be calculated using Equation 29 from Durst, Melling and Whitelaw (Durst, 1981).

$$\Delta y = y'\left[\frac{\sqrt{m_2^2 - \sin^2\alpha_1}}{\sqrt{1-\sin^2\alpha_1}} - 1\right] \qquad \text{Equation 29}$$

Δy is the change in position of the intersection point caused by refraction, y' is the location without refraction, m_2 is the refractive index of the fluid and α_1 is the half angle between the beams.

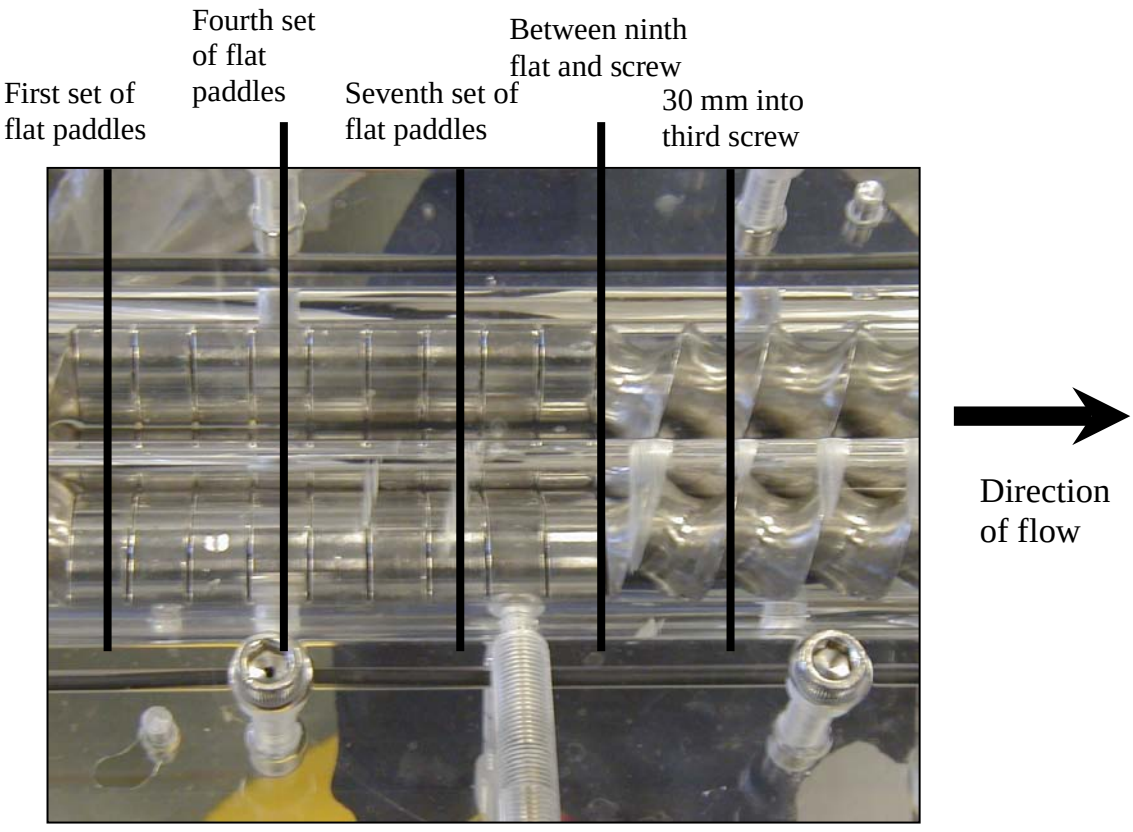

Figure 12 Top view of paddle arrangement in barrel

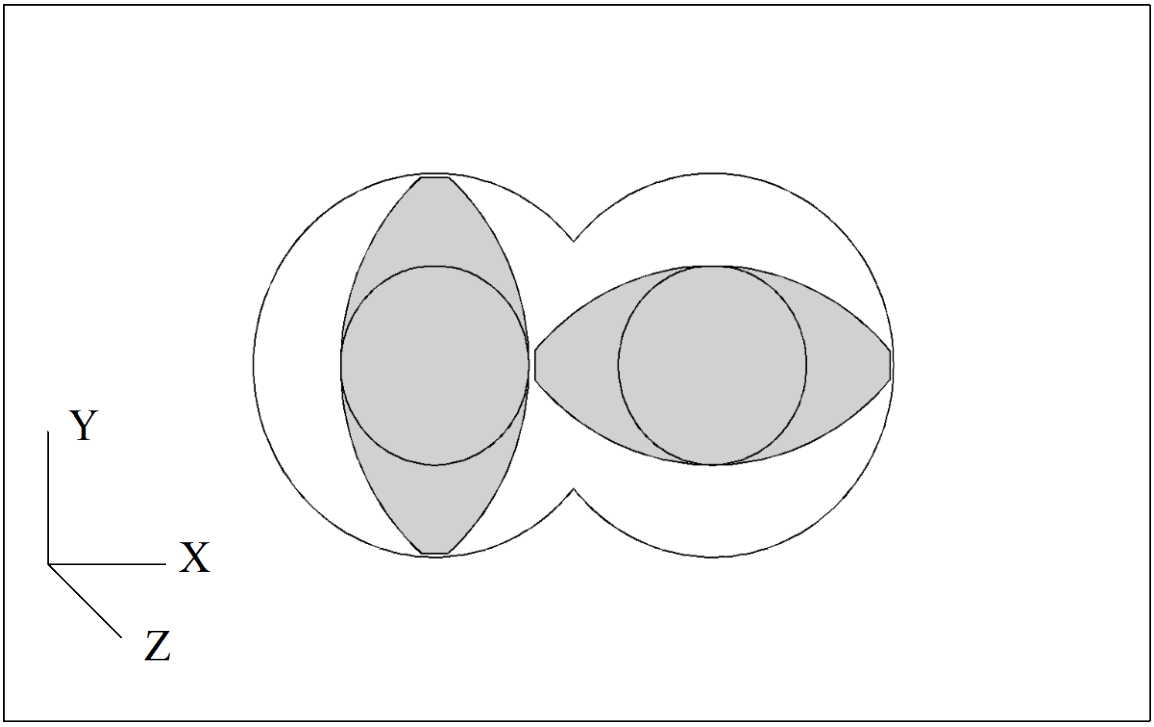

Figure 13 Paddle position at 0˚ from front of mixer

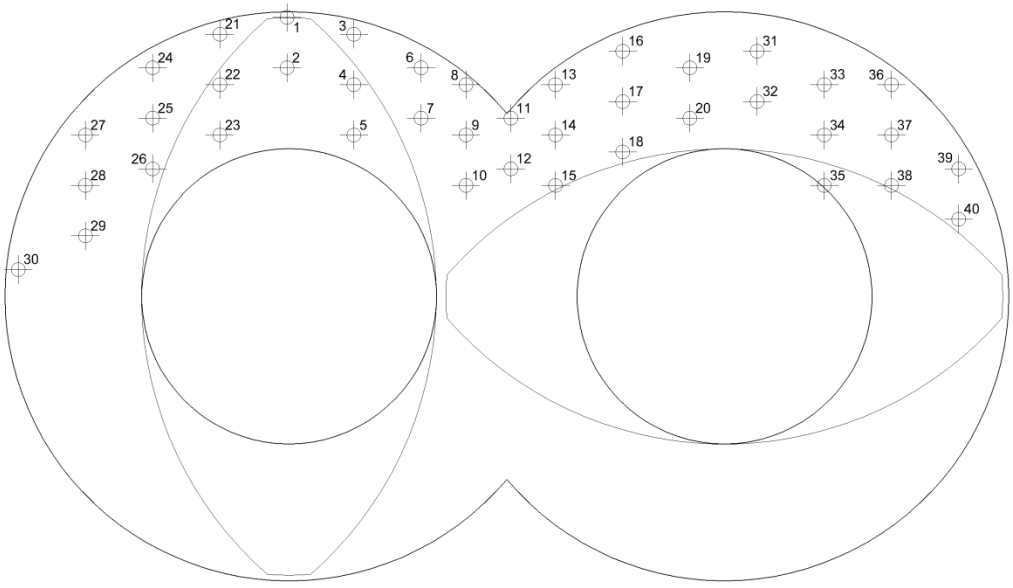

Figure 14 Points where measurements were taken

IV. Results

A. Couette Measurement Results

The results for the couette measurements are shown in Figure 15. The calculated velocity line falls within the error bounds of the refraction corrected measured velocity values. The couette measurements were done to determine that the experiments could be done accurately. The difference between the predicted and measured values decreases the closer the point comes to the wall of the outer cylinder. Some error is apparent in these results. The error could be caused by several sources. In order for the couette to strictly follow the equation used to calculate the velocity, it needs to be exactly centered in the outer cylinder. Great care was taken to center the bob; however there was some wobble in it which was measured to be less than 0.0015″. The couette was measured with calipers to make sure that it was centered in the cylinder. More error would also be caused by the centering of the lasers. They must intersect on the axis of the couette or the measured quantities will not be the tangential and axial velocities as expected but components of each instead.

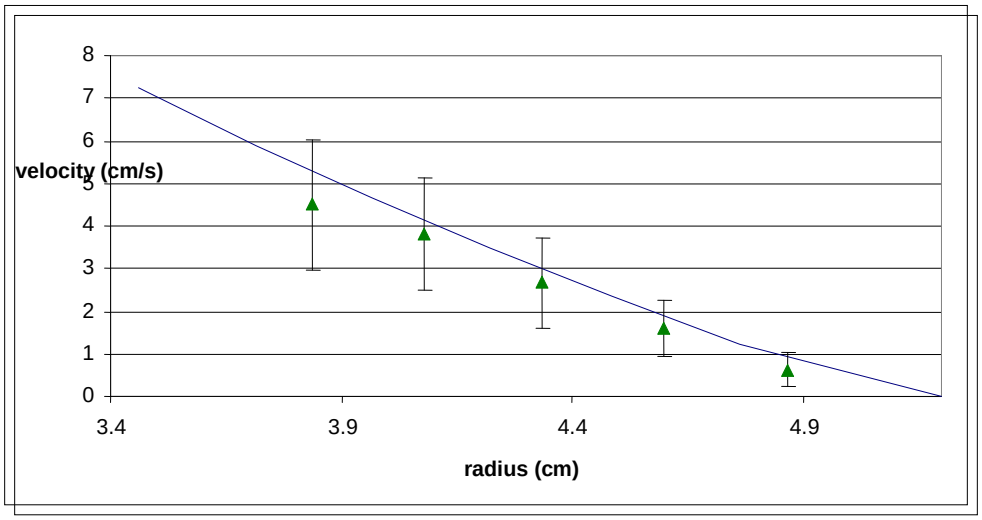

Figure 15 Results for Couette flow measurements

B. Determination of Velocity

Velocity was measured at 40 locations within the mixer operating at 100 rpm. The measured velocity is periodic, repeating every 180˚. Because of the symmetry of the paddles of the mixer, the mixer is back in its starting position after half a rotation of the shafts. This is shown in Figure 16. The velocity peaks every 180˚, starting at approximately 25˚. Measurements are not able to be taken for every encoder position because the lasers were blocked by the rotating paddles at some positions. The lack of measurements shows itself as breaks in the velocity profile. In Figure 16 the paddles pass over the measurement point around encoder position 135° and 315°. The velocity measurements were sorted by encoder position and then averaged for each position. X and Z velocity values for corn syrup are shown in Table 2.

The barrel can be divided into 3 regions: the middle region, the outside left region and the outside right region. The middle region is the section between the two paddles where the two shafts open into each other. It is made up of points 8 through 15. These points will experience the effect of both paddles sometime during the rotation. The intermeshing region is a subsection of the middle region where both paddles will cross the points. Measurements taken in this area were at points 10, 11, 12 and 15. The outside left region is made up of the points in the left barrel and not in the section open to the right barrel. Points measured in this area are points 1 through 7 and points 21 through 30. The outside right region is made up of the points in the right barrel that are not exposed to the left barrel. The points measured in this area are points 16 through 20 and 31 through 40.

All the points measured are affected by both paddles for at least part of the rotation. The effects of both paddles are felt when the barrel is open to the other side. When the paddle on the side the point is located totally closes the opening to the other side it eliminates the effect of the other paddle during the time that it is blocked off. An example of this is looking at point 24 at the 0˚ starting position of the paddles. In this position point 24 is blocked off from the right side of the barrel by the left paddle. It will not feel the effects of the right paddle until the left paddle passes over it and leaves it exposed to the right barrel.

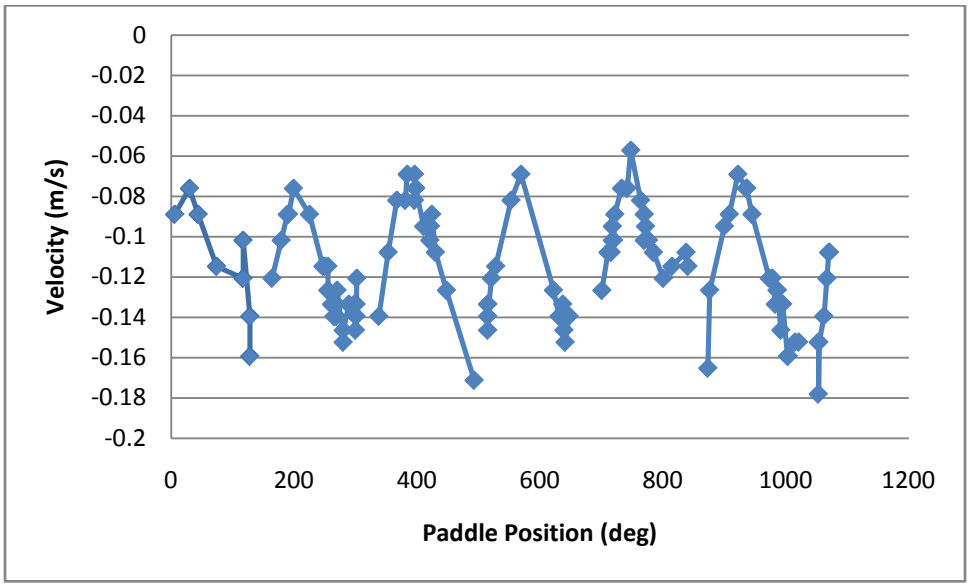

Figure 16 Carbopol X Velocity point 6 - 1st paddle

Table 2 X and Z Velocities of Corn Syrup at select positions

	0° Rotation		40° Rotation	
Point	X Velocty	Z Velocity	X Velocty	Z Velocity
1	0.02224	0.005645	-	-
2	-	-	-0.225605	0.013915
3	-0.00074	0.00729	-0.02891	0.00729
4	-	-	-0.2261	0.06862
5	-	-	-0.178751	-0.00376364
6	-0.044975	0.008935	-0.03595375	0.01481125
7	-0.181973	-0.246396	-0.167659	-0.00661934
8	-0.00616046	-0.0953438	-0.0152416	-0.00153412
9	-0.21582	-0.403439	-0.10799	0.0474
10	-0.122551	0.0534259	-	-
11	-0.12083	-0.06042	0.052306667	0.027663333
12	-0.315223	-0.28475	-0.20386	0.07098
13	-0.10799	-0.09333	-0.0472	0.024215
14	-0.384431	-0.307548	-0.155684	0.0399207
15	-0.104938	-0.00699802	-0.137562	0.034578
16	-0.155425	-0.002585	0.071746667	0.046783333
17	-0.340739	-0.391318	-0.19561	0.0525221
18	-0.193054	-0.0882103	-0.176832	0.0354373
19	-0.27404	0.0474	-0.19101	0.02759
20	-0.295694	-0.323558	-0.21572	0.030265
21	-0.12677	-0.002585	-0.04275	0.00729
22	-	-	-	-
23	-	-	-	-
24	-0.12677	0.00729	-	-
25	0.231536667	0.023188333	-	-
26	-0.127526	0.0181157	-	-
27	-0.10799	0.02798	-0.150348	0.00237509
28	-0.10291	0.0632081	-	-
29	-0.0622927	0.0627531	-0.0508208	0.017128
30	-0.02199	0.02759	-0.02891	0.02759
31	-0.11227	0.021863333	0.143988571	0.024617143
32	-0.293456	-0.366778	-0.216216	0.0162714
33	-0.19694	0.02759	-0.228968	0.020988
34	-0.229323	-0.199171	-	-
35	-	-	-	-
36	-0.01161	-0.002585	0.4119275	-0.0009425
37	-0.207453	-0.190498	-	-
38	-0.124316	-0.0339601	-	-
39	0.019683333	0.003683333	0.038231429	0.001648571
40	-0.13961	0.04079	-0.066475	0.017685

Table 3 X and Z Velocities of Corn Syrup at select positions (continued)

	80° Rotation		120° Rotation	
Point	X Velocty	Z Velocity	X Velocty	Z Velocity
1	-	-	-	-
2	-0.2181925	0.075695	-0.24142	0.01438
3	-0.03616	0.01387	-0.0237225	0.004
4	-0.264155	0.08324	-0.35509	0.017685
5	-0.245447	0.284546	-	-
6	0.052306667	0.014028333	-0.010135	0.003683333
7	-0.25427	0.055415	-	-
8	-0.0338949	0.0867074	-	-
9	-0.2404325	0.05164	-0.49347	-0.00637
10	-	-	-	-
11	-0.06351	0.02798	-0.137635	0.030951667
12	0.281286667	0.08481	-	-
13	0.070428571	0.019781429	-0.16531	-0.00588
14	-0.17816	0.0474	-	-
15	-0.138563	0.459073	-	-
16	0.135234286	0.01105	-	-
17	-0.24142	0.03419	-	-
18	-	-	-	-
19	-	-	-	-
20	-	-	-	-
21	-0.04374	0.01387	-0.04374	0.00729
22	-0.24834	0.054	-0.22956	0.04079
23	-0.184148	0.0857787	-0.216436	0.162378
24	-0.079325	0.0364375	-0.072208	0.018008
25	-0.27997	0.02099	0.18244333	0.050853333
26	-	-	-0.23549	0.01438
27	-0.13961	0.00729	-0.08921	0.02045
28	-	-	-0.14653	0.02759
29	-	-	-0.104936	0.0960106
30	-	-	-0.03583	0.02099
31	-	-	0.08525125	0.01481
32	-	-	-0.200698	0.00570022
33	-	-	-0.130225	0.040795
34	-	-	-0.20386	0.04079
35	-	-	-	-
36	-0.02545	0.00729	-0.01161	0.01058
37	-0.133484	0.00778	0.09909333	0.042993333
38	-0.114481	0.00645968	-0.130285	0.0824139
39	-0.01507	0.00729	0.01474333	0.011676667
40	-0.04374	0.01438	-0.05066	0.02759

Table 4 X and Z Velocities of Corn Syrup at select positions (continued)

	160° Rotation		200° Rotation	
Point	X Velocty	Z Velocity	X Velocty	Z Velocity
1	-	-	-0.0483062	0.00448769
2	-	-	-	-
3	-	-	-0.043245	-0.014575
4	-	-	-0.20979	0.02759
5	-	-	-	-
6	-	-	0.026603333	0.0029
7	-	-	-0.14653	0.01438
8	0.00375044	-0.132907	-0.0178805	0.00784451
9	-0.19101	0.0889	-0.10107	0.02759
10	-0.127386	0.0520309	-0.166119	0.0491071
11	-0.15592	-0.009635	-0.0688225	0.027663333
12	-	-	-0.195408	0.0516858
13	0.137636667	0.011676667	-0.0761125	-0.00282
14	-0.27756	-0.0604015	-0.189769	0.0451778
15	-	-	-0.166907	0.0433201
16	-0.15098	0.0293875	-0.11441	0.00729
17	-0.419384	-0.221347	-0.225037	0.0426401
18	-	-	-0.198902	0.0297247
19	-0.2859	0.07758	-0.20979	0.04079
20	-0.275817	-0.160444	-0.229869	0.0206332
21	-0.05066	0.00071	-	-
22	-0.267615	0.01108	-	-
23	-	-	-	-
24	-0.0778425	0.005645	-0.22843	0.018905714
25	-0.206825	0.020985	-	-
26	-0.150007	0.0405782	-	-
27	-0.09514	0.02798	-0.13961	0.002903333
28	-0.13368	0.02759	-0.13368	0.02759
29	-0.0714913	0.0422862	-0.0512494	0.00797102
30	-0.00736691	0.0101318	-0.02199	0.02759
31	-0.15246	0.03205	-0.159578	0.004654
32	-0.316192	-0.363974	-0.218405	0.00728991
33	-0.17816	0.07098	-0.21671	0.03419
34	-0.247358	-0.295608	-	-
35	-	-	-	-
36	0.024296667	0.009483333	-0.02891	0.005096667
37	-0.15592	0.08607	0.250646667	0.012966667
38	-0.174004	-0.190219	-	-
39	0.016498889	0.01387	-0.09514	-0.00588
40	-0.08229	0.04079	-	-

Table 5 X and Z Velocities of Corn Syrup at select positions (continued)

	240° Rotation		280° Rotation	
Point	X Velocty	Z Velocity	X Velocty	Z Velocity
1	-0.0426522	0.0139929	-0.0702569	-0.00487764
2	-0.229065	0.06249	-0.2510575	0.115545
3	0.013595	0.01058	-0.0343475	0.00729
4	-0.20979	0.054	0.335983333	0.081666667
5	-	-	-0.153515	-0.00249122
6	-0.046705	0.005645	0.066803333	0.020766667
7	-0.199345	0.00523902	-0.38969	0.0474
8	-0.0454521	0.00728455	-0.0100321	-0.0139868
9	-0.15279	0.077266667	0.402985455	0.070207273
10	-	-	-	-
11	-0.04374	-0.02798	0.105683333	0.030951667
12	-	-	-0.38969	0.02759
13	-0.05659	0.01716	-0.12281	0.019121667
14	-0.15938	0.08324	-0.20386	0.054
15	-	-	-0.242401	-0.0584224
16	-0.096524	0.016502	-0.23549	-0.01246
17	-0.22264	0.07098	-	-
18	-	-	-	-
19	-0.251305	0.03419	-	-
20	-	-	-	-
21	-0.04374	0.01387	-0.04374	0.02798
22	-0.27404	0.03419	0.252293333	0.08544
23	-	-	-	-
24	0.127093333	0.00729	-0.08229	-0.03315
25	-0.27997	0.03419	-0.22956	0.02099
26	-	-	-0.25427	0.00778
27	-0.11392	0.02045	-0.11392	0.04772
28	-	-	-0.17816	0.054
29	-	-	-	-
30	-0.02891	0.01438	-0.06351	0.00778
31	-0.27218625	-0.01187125	-0.19553	0.002115714
32	-	-	-	-
33	-	-	-0.12459	0.02627
34	-	-	-0.169226	-0.00508295
35	-	-	-	-
36	-0.04411	0.00071	-0.019222	0.007948
37	-	-	-0.11392	0.02099
38	-	-	-	-
39	-0.02199	0.00729	-0.01507	0.011676667
40	-0.05066	0.01438	-0.04374	0.02099

Table 6 X and Z Velocities of Corn Syrup at select positions (continued)

	320°Rotation		360°Rotation	
Point	X Velocty	Z Velocity	X Velocty	Z Velocity
1	-0.0523393	0.0440651	-0.00815	-0.00588
2	-0.23549	0.02649	-	-
3	-0.05313	-0.0009375	0.025855455	0.001305455
4	-0.2814525	0.01108	-	-
5	-	-	-	-
6	0.084596667	-0.00149	-0.04275	0.011676667
7	-	-	-0.195951	-0.057347
8	-	-	-0.00335728	-0.0190913
9	-	-	-0.15938	0.01438
10	-	-	-0.217501	-0.0805462
11	-0.0543625	0.009635	-0.11392	0.027663333
12	-	-	-0.397203	-0.070301
13	0.272204286	0.029517143	-0.13319	-0.033145
14	-	-	-0.470088	-0.0895385
15	-	-	-0.121576	-0.00360514
16	0.145048333	0.008386667	-0.184585	0.020925
17	-	-	-0.420655	-0.129096
18	-	-	-0.228794	-0.0365787
19	-0.229065	0.03419	-0.49347	0.02759
20	-	-	-0.352975	-0.112364
21	0.033853333	0.00729	-0.110955	0.004
22	-0.21325	0.03419	-	-
23	-0.24142	0.02099	-	-
24	-0.0679575	0.012225	0.125113333	0.005096667
25	-0.17124	0.03419	-0.22956	0.02759
26	-0.186917	0.112943	-0.129275	0.0107497
27	-0.08229	0.02045	-0.10799	0.03456
28	-0.12677	0.03749	-0.108959	0.0454123
29	-	-	-0.0655922	0.0511623
30	-0.03237	0.02429	-0.0069379	0.017906
31	-0.19101	0.02798	-0.146728	-0.05139
32	-0.26119	0.06532	-0.347194	-0.134869
33	-0.13105	0.04708	-0.21325	0.045985
34	-0.166932	0.0103193	-0.190037	0.0285712
35	-	-	-	-
36	-0.01853	0.00729	-0.00025	0.01387
37	-0.11565	0.0308925	-0.223682	-0.0765243
38	-0.133819	0.0526203	-0.126127	-0.0128982
39	-0.01507	0.00729	-0.02199	-0.01392111
40	-0.05066	0.02759	-0.13961	0.01438

Figure 17, Figure 18, and Figure 19 show a cross section of the measurement results for the x velocity taken at the fourth flat paddle with a paddle position of 0˚ for each fluid with the mixer operating at 100 rpm. The figures show similar velocity trends among the three fluids. The x velocities are highest in the middle of the barrel above the left half of the right paddle. The velocities decrease around the edge of the barrel and left half of the center section of the barrel. The range of velocity for CMC and Carbopol in this position are close in value with a range of -0.0197 to -0.2800 m/s for CMC and a range of -0.0325 to -0.2918 m/s for Carbopol. The range for the corn syrup velocities is -0.0208 to -0.3408 m/s.

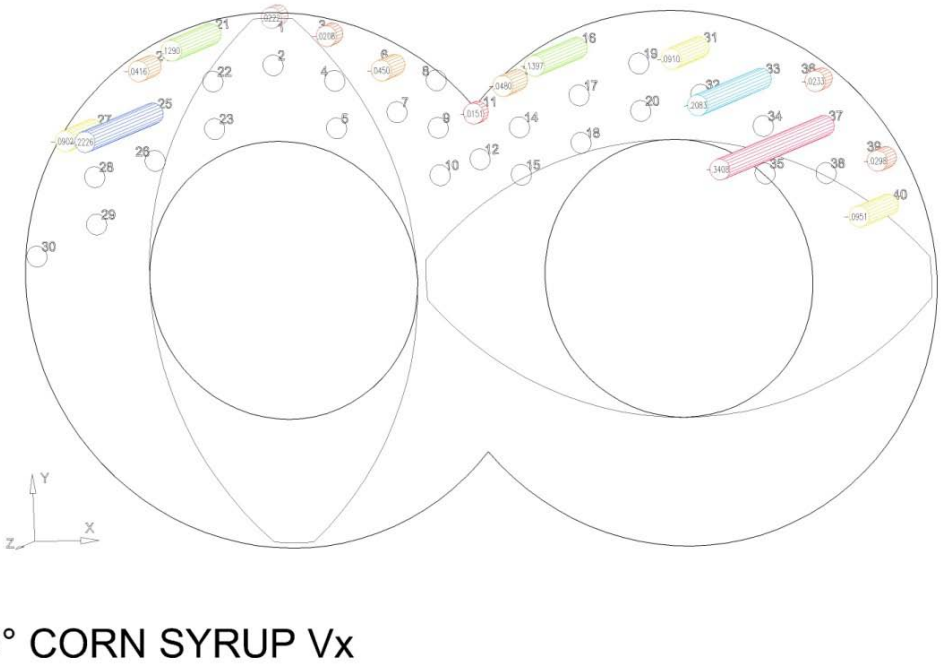

Figure 17 Corn Syrup X Velocity at 0 degrees rotation at 100 rpm

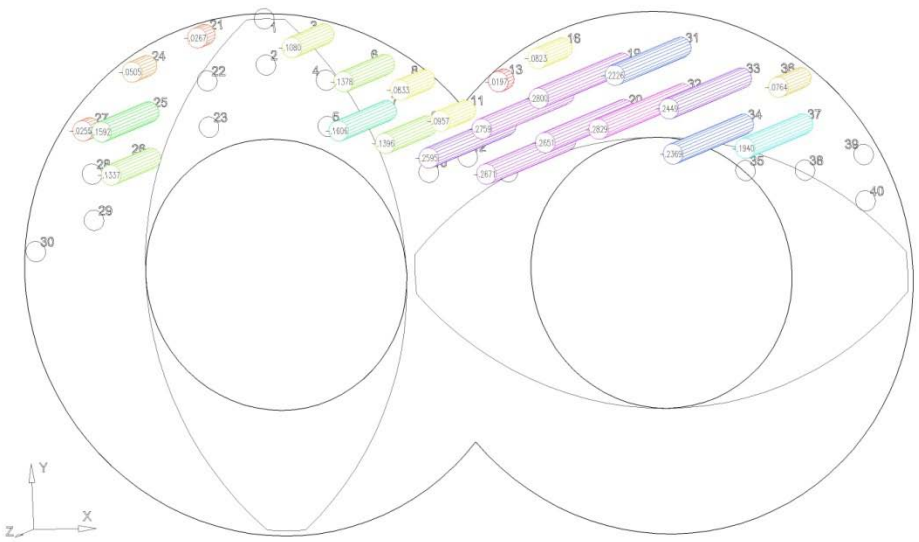

Figure 18 CMC X Velocity at 0 degrees rotation at 100 rpm

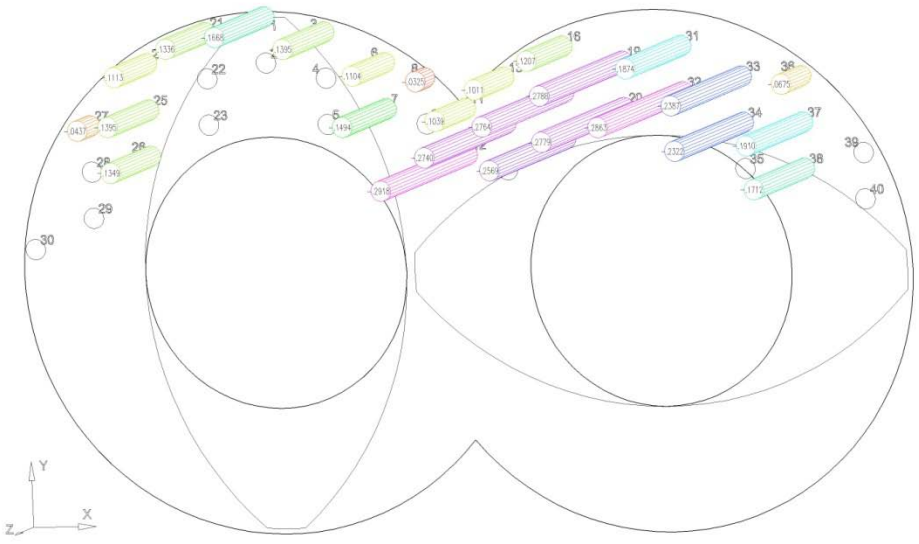

Figure 19 Carbopol X velocity at 0 degrees rotation at 100 rpm

Cross sections showing the z velocity at the fourth flat paddle at 0˚ rotation are shown in Figure 20, Figure 21, and Figure 22 for each of the fluids. The z velocity trends follow those of the x velocity with the highest velocities being in the center of the barrel over the right paddle. For the velocity ranges at this location and paddle position there is an order of magnitude difference between the corn syrup velocity range and those of the CMC and Carbopol. The range for the corn syrup velocities is 0.0002 to 0.0427 m/s, the range for CMC is 0.0070 to 0.1004 m/s and the range for Carbopol is 0.0040 to .1070 m/s. In the section with the highest velocities, the velocities of the Carbopol tend to be slightly higher than those of the CMC and corn syrup at the same location.

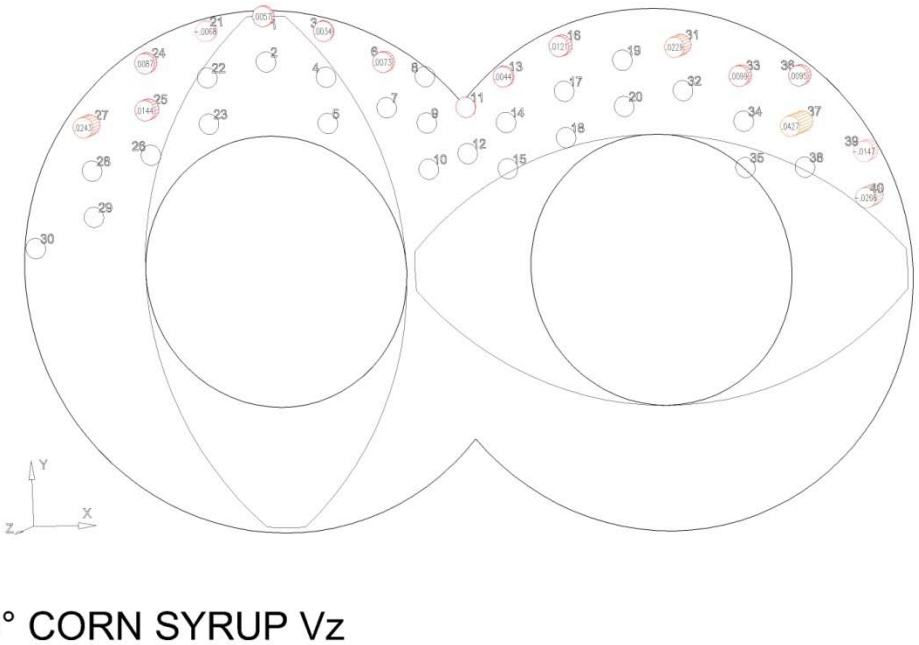

Figure 20 Corn Syrup Z Velocity at 0 degrees rotation at 100 rpm

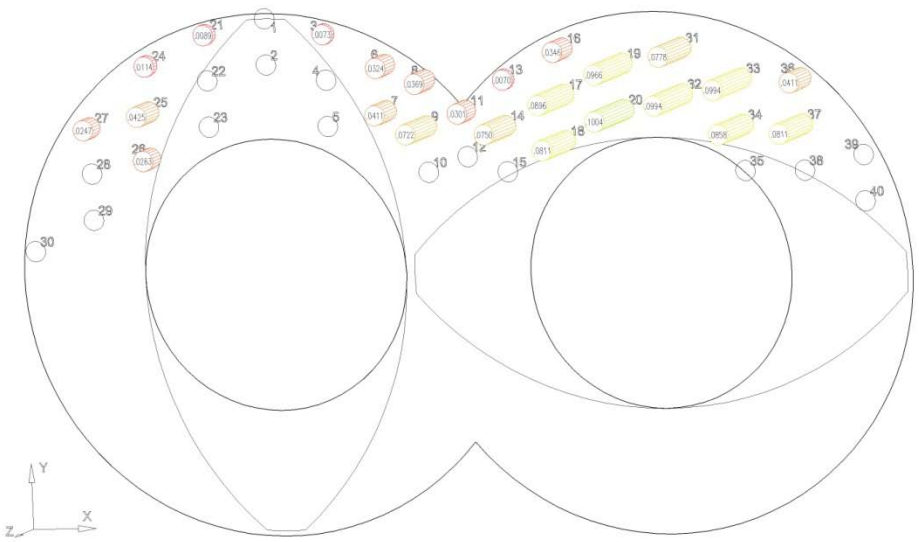

0° CMC Vz

Figure 21 CMC Z Velocity at 0 degrees rotation at 100 rpm

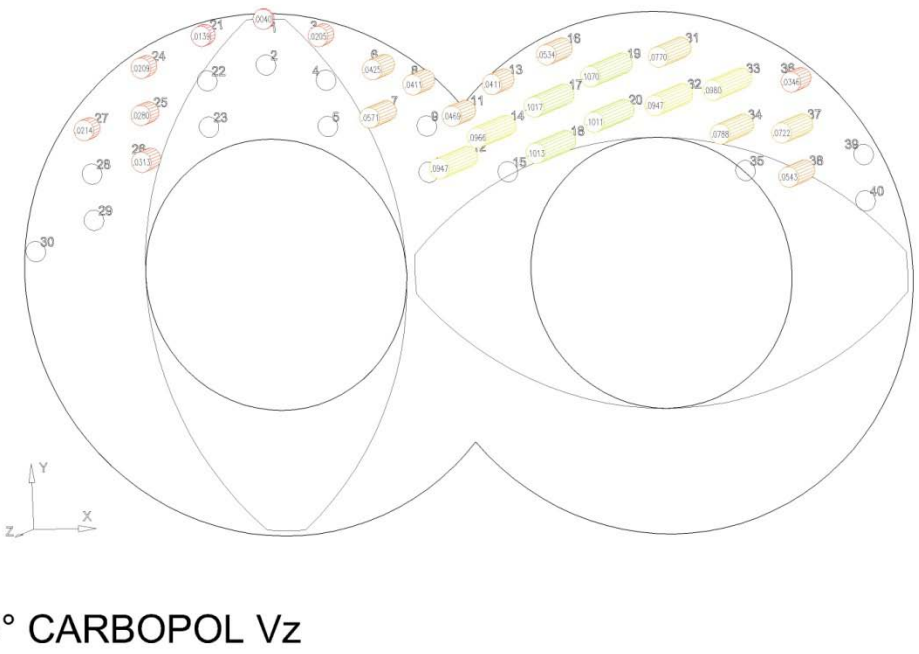

Figure 22 Carbopol Z Velocity at 0 degrees rotation at 100 rpm

The cross sections of the fourth flat paddle at 45˚ rotation are shown for the x velocity in Figure 23, Figure 24 and Figure 25. At this rotation both the left and the right sides of the barrel are cut off from the center by the paddles. The highest velocities are throughout the center section of the mixer closer to the paddles. The highest velocities for each fluid are lower for this position of the paddle than they were for 0˚ rotation. The range for corn syrup at this position is -0.0222 to -0.2097 m/s, the range for CMC is -0.0309 to -0.2381 m/s and the range for Carbopol is -0.0151 to -0.2353 m/s.

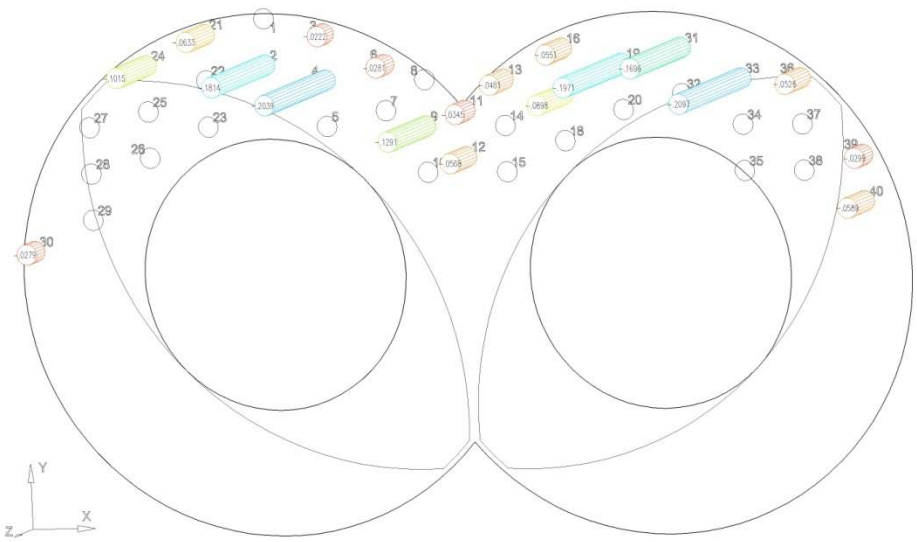

Figure 23 Corn Syrup X Velocity at 45 degrees roation

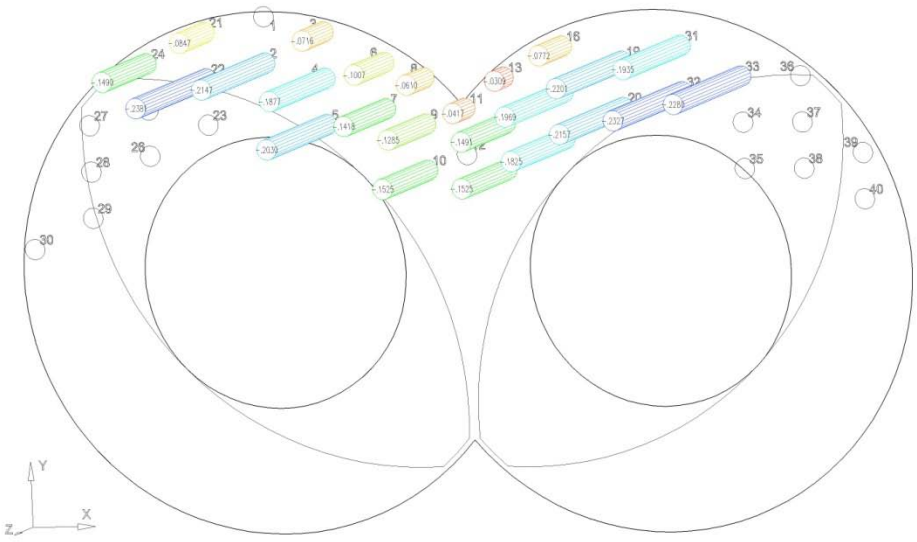

Figure 24 CMC X Velocity at 45 degrees rotation

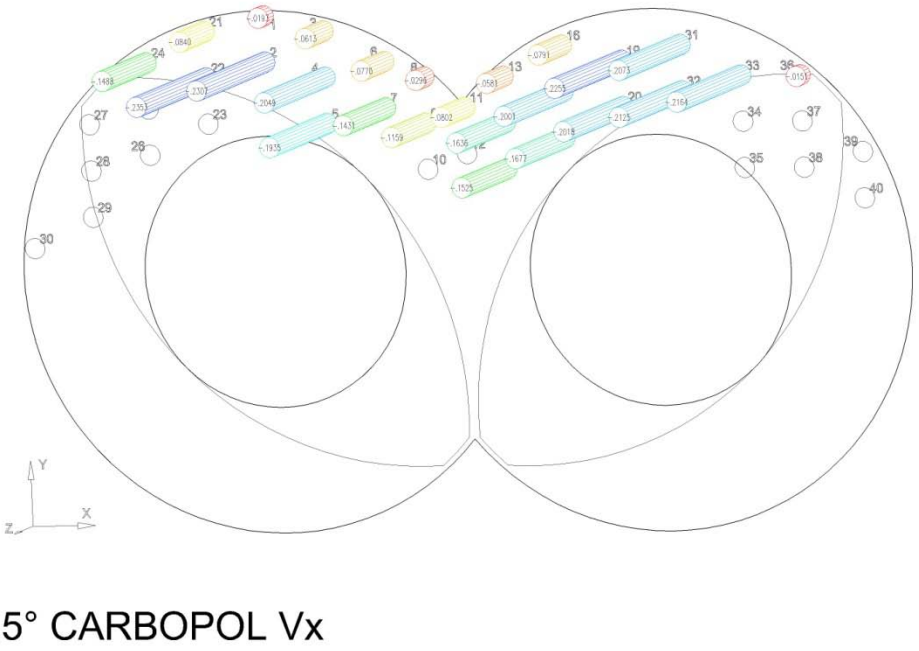

Figure 25 Carbopol X Velocity at 45 degrees rotation

The z velocity cross sections at 45˚ rotation are shown in Figure 26, Figure 27 and Figure 28. The z velocities are similar to those for 0˚ rotation with ranges of 0.0007 to 0.0654 m/s for corn syrup, 0.0173 to 0.0656 m/s for CMC and 0.0063 to 0.0670 m/s for Carbopol. The maximum velocities for each fluid are within 0.002 m/s of each other. The highest velocities are in the center of the barrel away from both the outer wall and paddle edge.

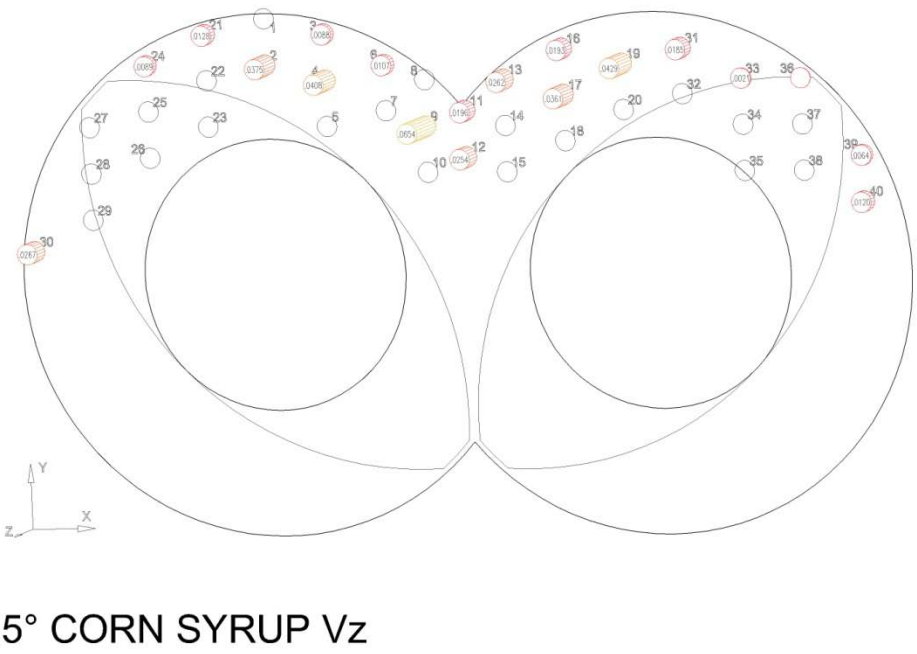

Figure 26 Corn Syrup Z Velocity at 45 degrees rotation

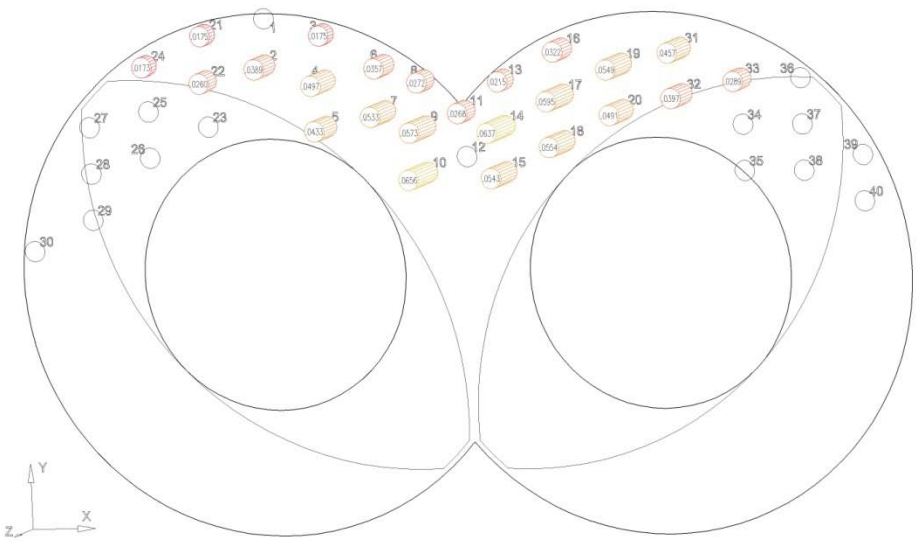

Figure 27 CMC Z Velocity at 45 degrees rotation

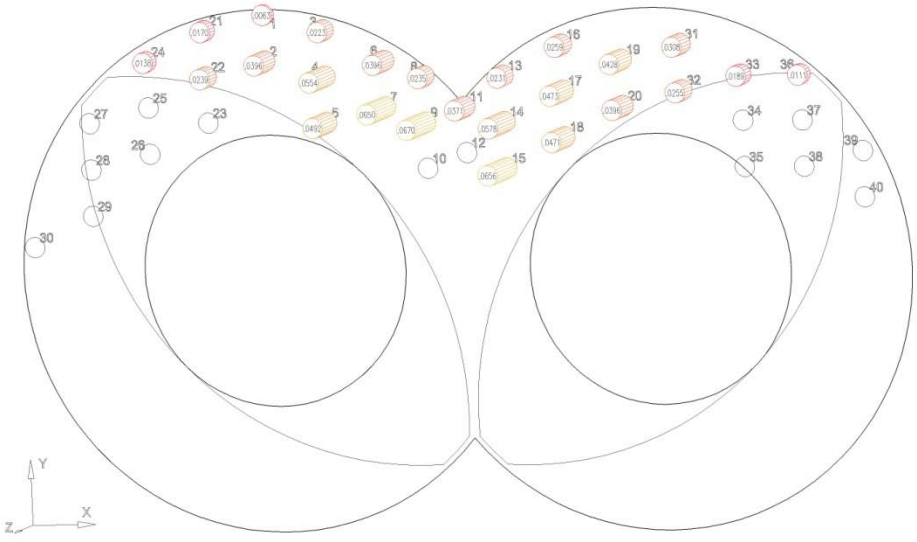

Figure 28 Carbopol Z Velocity at 45 degrees rotation

Cross sections for the three fluids at 90˚ rotation are shown in Figure 29, Figure 30, Figure 31, Figure 32, Figure 33 and Figure 34. The x velocity ranges for all three fluids are close to the values at 0˚ rotation of the paddles. The ranges are -0.0133 to -0.3520 m/s for corn syrup, -0.0123 to -0.2681 m/s for CMC and -0.0082 to -0.2740 m/s for Carbopol. The highest velocities are located in the left half of the mixer closer to the paddles. For the z velocities, the corn syrup is higher than both the CMC and Carbopol which are both close in ranges. The ranges for z velocity are 0.0058 to 0.0985 m/s for corn syrup, 0.0039 to 0.0288 m/s for CMC and 0.0059 to 0.0389 m/s for Carbopol.

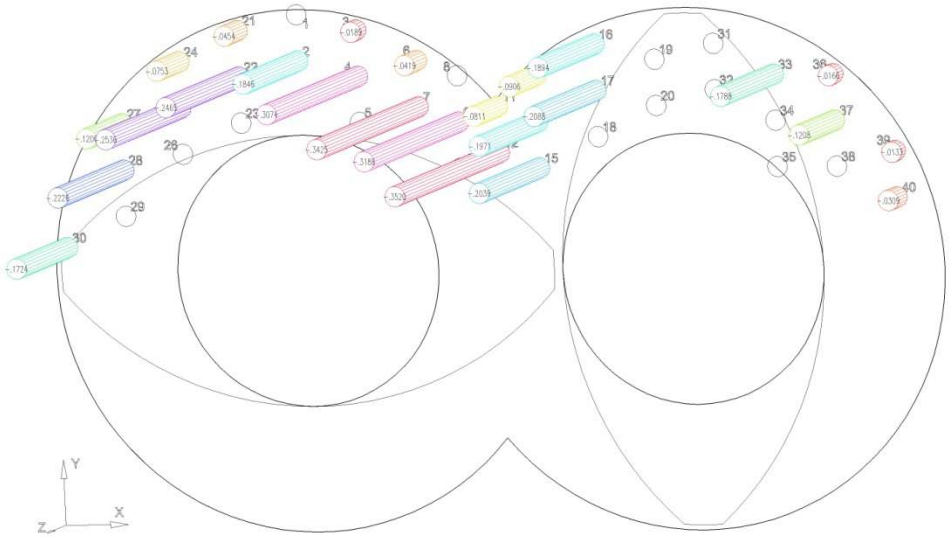

Figure 29 Corn Syrup X Velocity at 90 degrees rotation

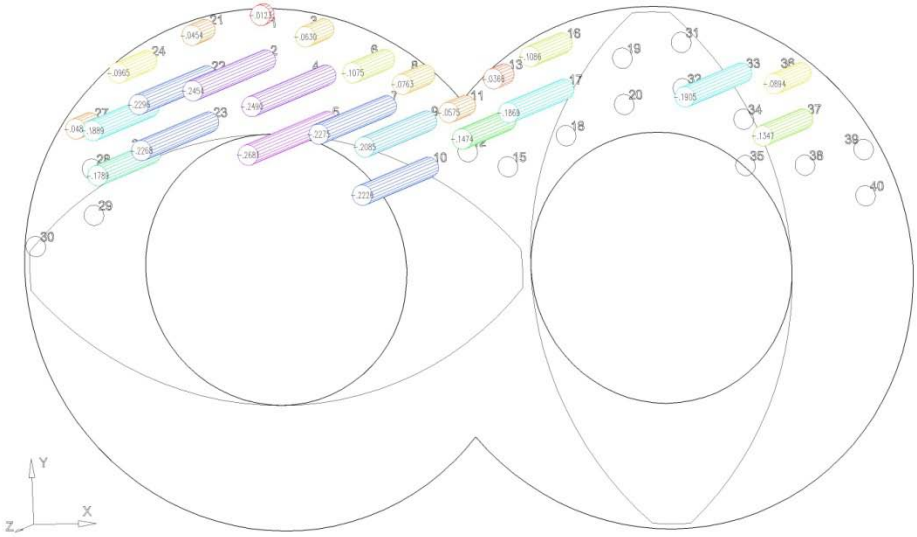

Figure 30 CMC X Velocity at 90 degrees rotation

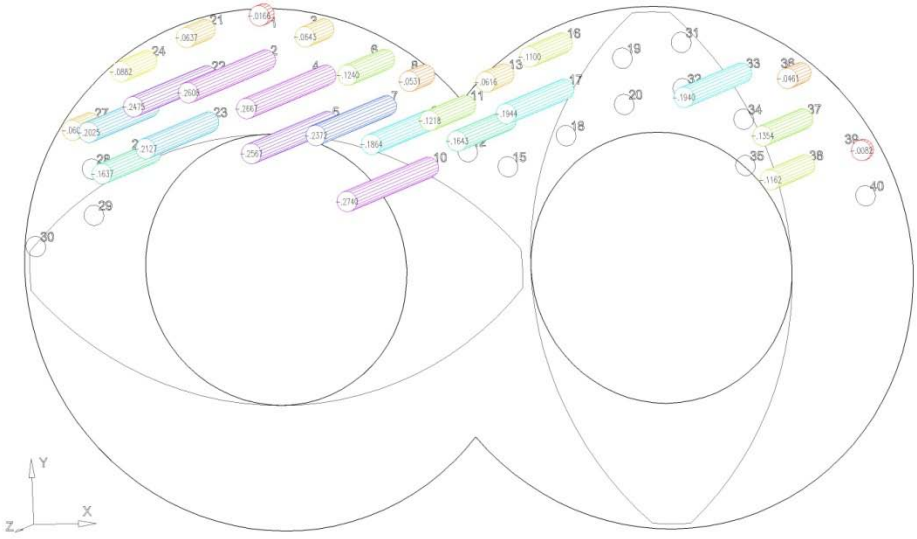

Figure 31 Carbopol X Velocity at 90 degrees rotation

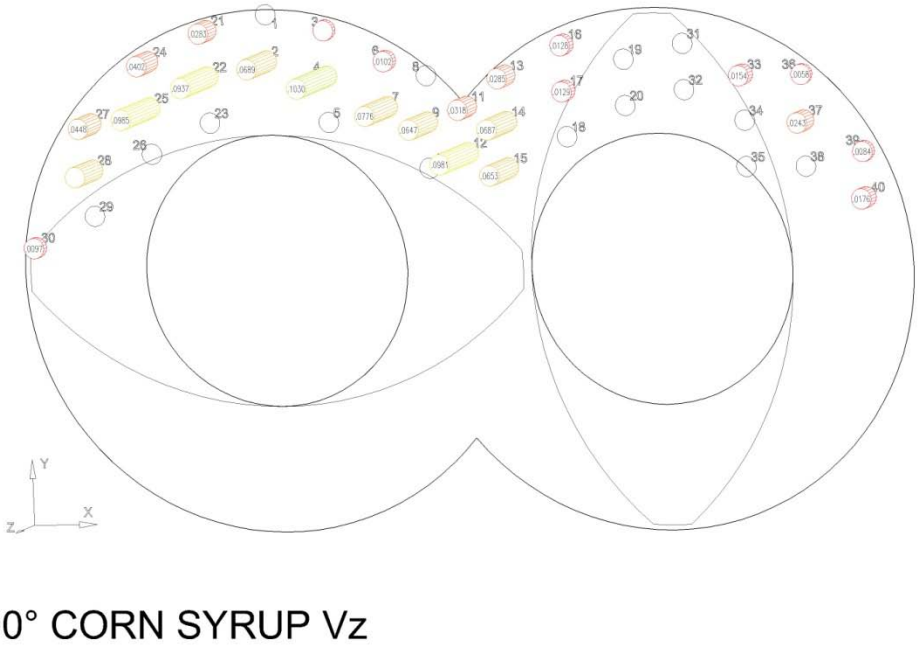

Figure 32 Corn Syrup Z Velocity at 90 degrees rotation

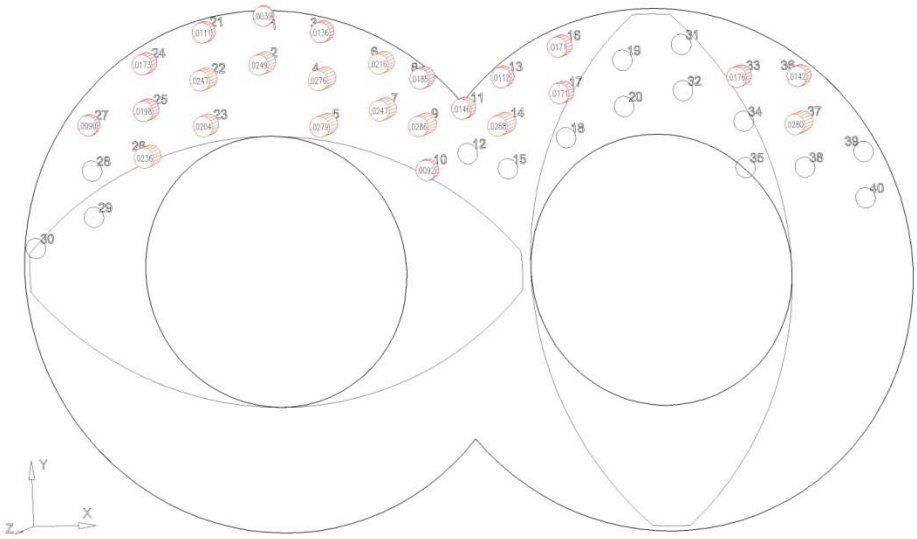

Figure 33 CMC Z Velocity at 90 degrees rotation

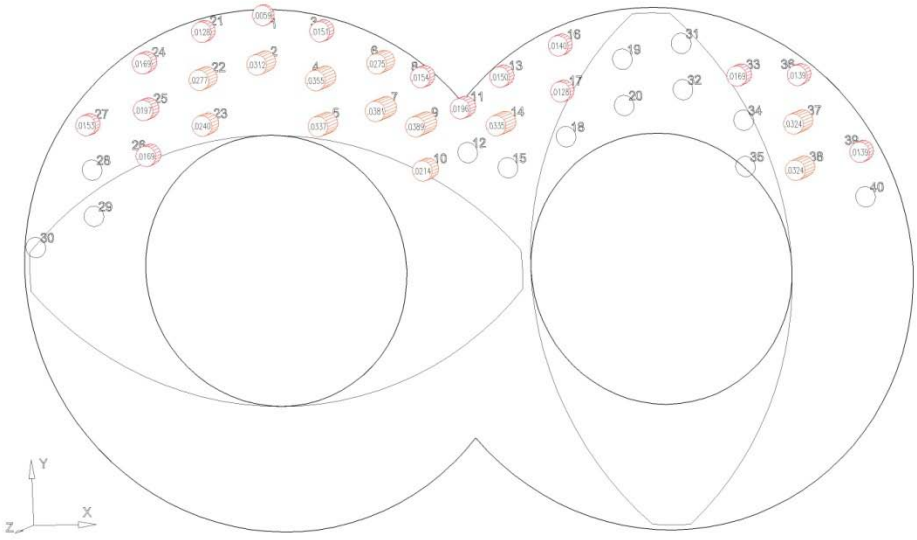

Figure 34 Carbopol Z Velocity at 90 degrees rotation

Figure 35, Figure 36, and Figure 37 show direct comparisons of the measurements of the three different fluids at different measurement points within the mixer. From these graphs, it can be seen that at the different points the x velocities fall roughly within the same range for each of the points. The z velocities fall into another smaller range. The curves of the CMC and Carbopol more closely follow each other than the corn syrup curve. In each of the cases the CMC and Carbopol overall have a higher velocity magnitude than the corn syrup. For the z velocity curves, the CMC and Carbopol do not experience the same backflow that the corn syrup does.

It is not surprising that the behavior of CMC and Carbopol follow each other much closer than corn syrup since they are both shear thinning fluids. Since they are shear thinning their viscosities will decrease when increasing shear is applied to them. In the mixer, shear increases as the fluid passes between the tip of the paddle and the barrel wall. These high shear areas are where the velocities are greatest. The corn syrup had a higher viscosity than the CMC or Carbopol throughout the experiments.

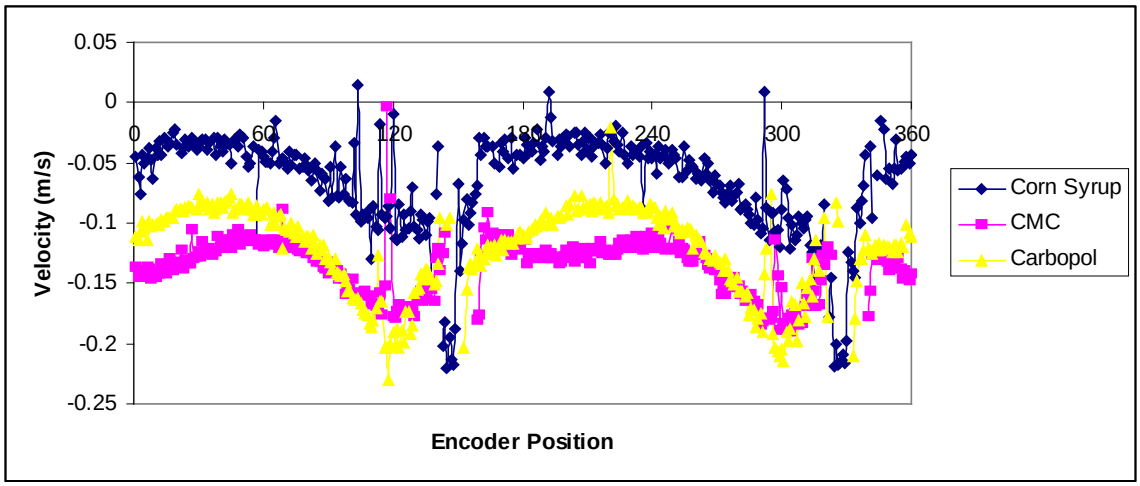

a) X velocity

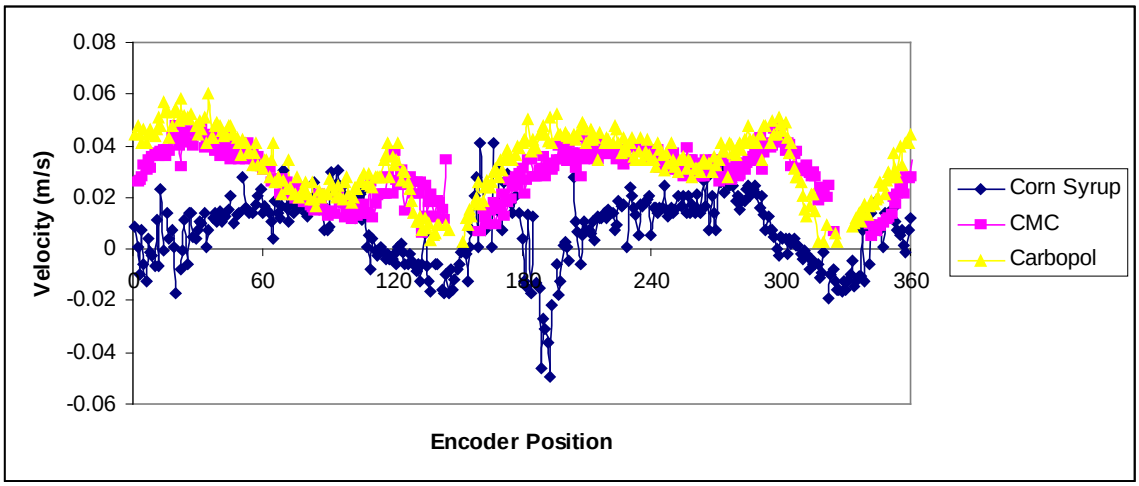

b) Z velocity

Figure 35 Comparison of fluids at pt 6 4th flat paddle

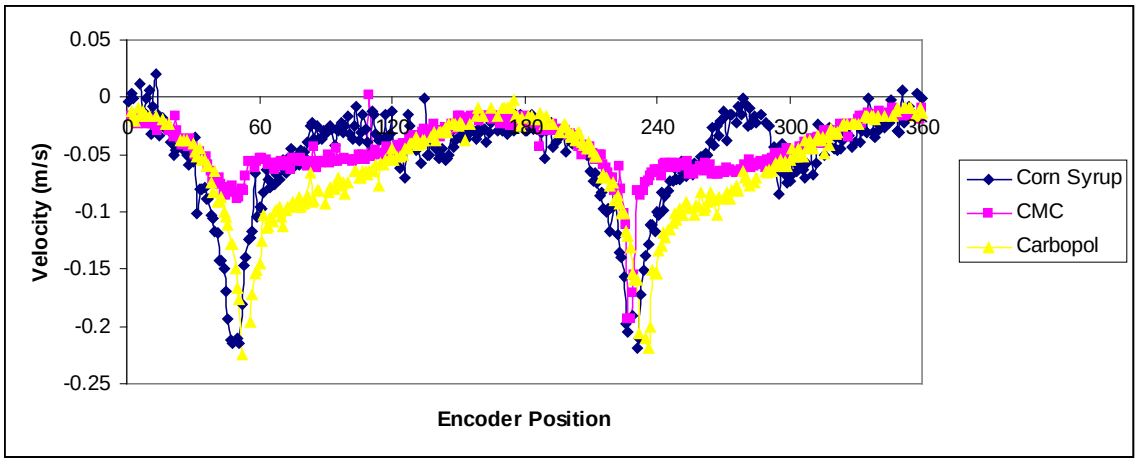

a) X velocity

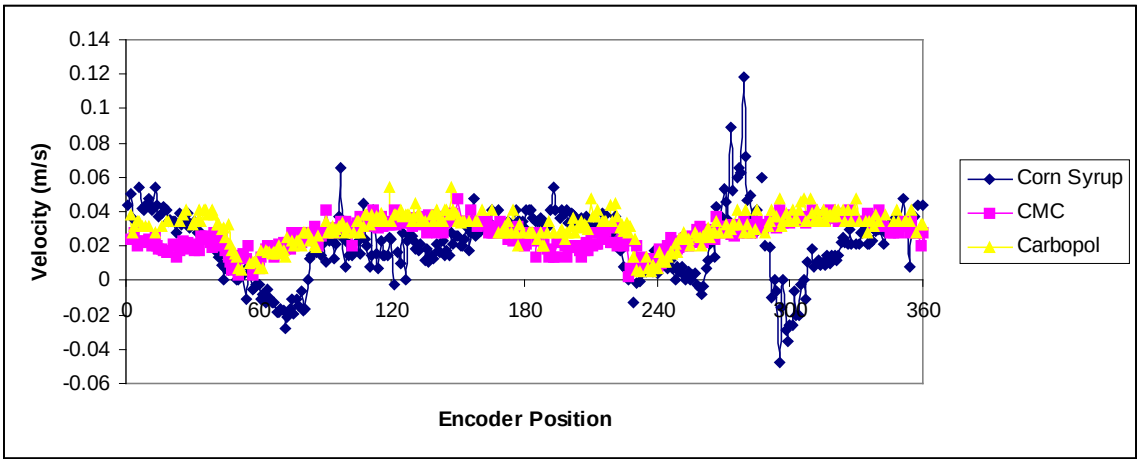

b) Z velocity

Figure 36 Comparison of fluids at pt 6 30mm into screw

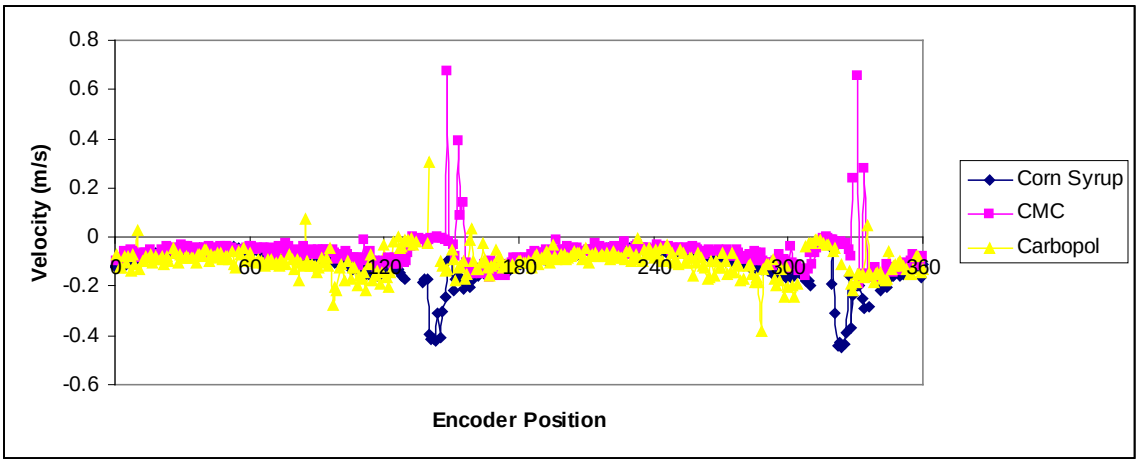

a) X velocity

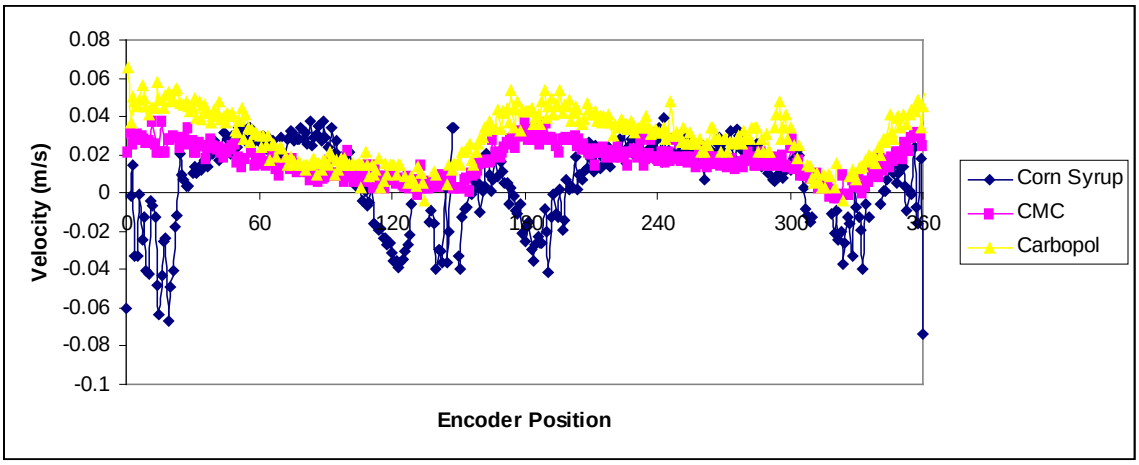

b) Z velocity

Figure 37 Comparison of fluids at pt 11 4th flat paddle

C. Comparison with Computer Simulations

Computer simulations were performed by Ashoken (2008) to simulate the paddle section of the continuous mixer. The simulations were done by the finite element method. These experimental results at the fourth flat paddle were compared to simulations of a set of five flat paddles. The simulation results compared were taken from the third paddle. Results comparing point 11 are shown in Figure 38 and Figure 39 for the x and z velocities respectively. For both velocities, the data follows the same general trends. The root mean square error is 0.123 for the x velocity and 0.021 for the z velocity. The maxima in Figure 38 for the x velocity fall within 0.005 m/s of each other.

The difference in values for the experimental and simulated data become greater at the minimums. The maximum values for the z velocity have a larger difference of 0.02 m/s but the overall accuracy is greater.

The error in the experimental measurements has several possible sources. If the lasers of the LDA were not centered correctly then all the measurements will be off. Great care was taken to center and line up the lasers each time measurements were taken but because measurements were taken over several days some small differences in set up could have occurred. The encoder also needed to be set to its zero location each time the system was setup. If it was not set precisely then it could cause some error in the measurements.

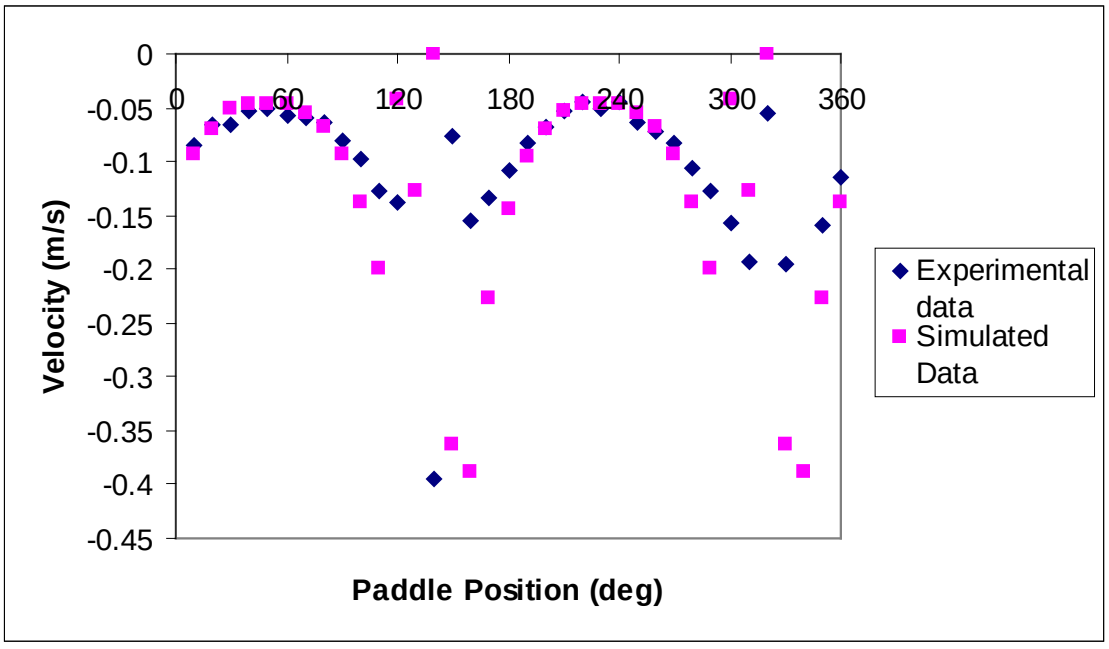

Figure 38 Comparsion between experimental and simulated X velocity results at point 11

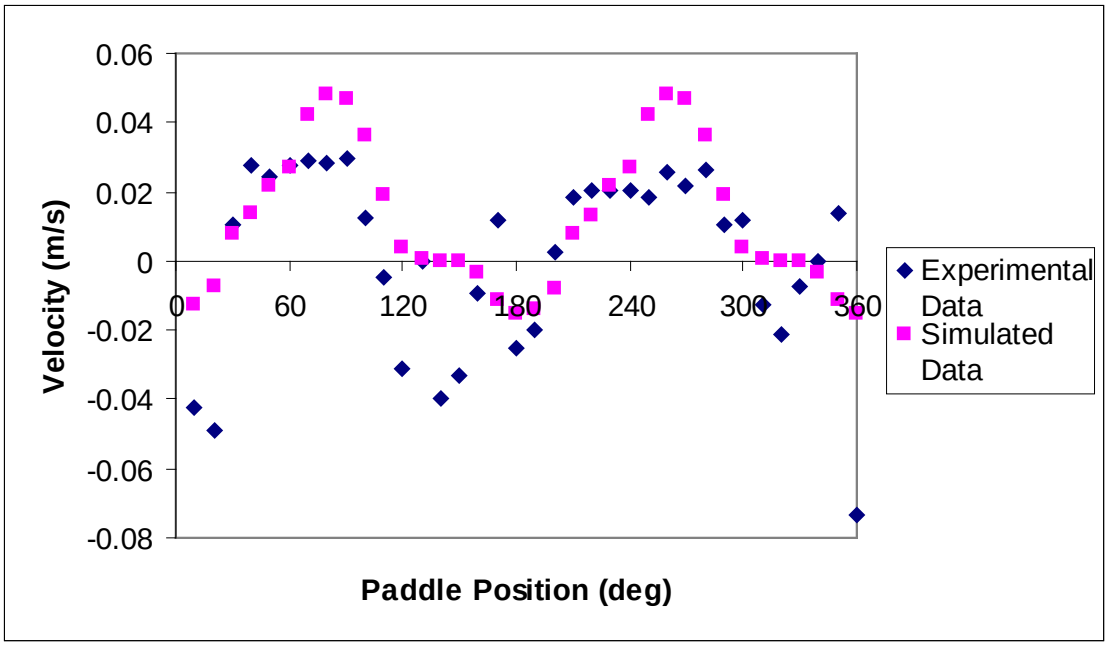

Figure 39 Comparison between experimental and simulated Z velocity results at point 11

D. Shear Rate

The shear rate is calculated as the square root of the second invariant of the strain rate tensor (Bird, Armstrong and Hassager, 1987). The strain rate tensor is

$$\overline{\overline{\Delta}} = \begin{bmatrix} 2\frac{dv_x}{dx} & \frac{dv_x}{dy}+\frac{dv_y}{dx} & \frac{dv_x}{dz}+\frac{dv_z}{dx} \\ \frac{dv_x}{dy}+\frac{dv_y}{dx} & 2\frac{dv_y}{dy} & \frac{dv_y}{dz}+\frac{dv_z}{dy} \\ \frac{dv_x}{dz}+\frac{dv_z}{dx} & \frac{dv_y}{dz}+\frac{dv_z}{dy} & 2\frac{dv_z}{dz} \end{bmatrix} \qquad \text{Equation 30}$$

The fluids used are incompressible, therefore I, the first invariant, is equal to zero. The second invariant, II, is given by the equation:

$$II = \frac{1}{2}\left(I^2 - \sum_m^3 \sum_n^3 \Delta_{mn}\Delta_{nm} \right) = \frac{1}{2}\left[I^2 - tr\left(\Delta_{im}\Delta_{mj}\right)\right] = \frac{1}{2}\left(I^2 - \overline{\overline{\Delta}} : \overline{\overline{\Delta}} \right) \qquad \text{Equation 31}$$

Since in this case the fluid is incompressible the equation becomes:

$$II = -\frac{1}{2}\left(\overline{\overline{\Delta}} : \overline{\overline{\Delta}}\right) \qquad \text{Equation 32}$$

When this is solved, II is shown to equal:

$$-II = 2\left[\left(\frac{dv_x}{dx}\right)^2 + \left(\frac{dv_y}{dy}\right)^2 + \left(\frac{dv_z}{dz}\right)^2\right] + \left(\frac{dv_x}{dy} + \frac{dv_y}{dx}\right)^2 + \left(\frac{dv_x}{dz} + \frac{dv_z}{dx}\right)^2 + \left(\frac{dv_y}{dz} + \frac{dv_z}{dy}\right)^2$$

Equation 33

where:

$$\dot{\gamma} = \sqrt{-II} \qquad \text{Equation 34}$$

Equation 33 and Equation 34 are used to find the shear rate for each measurement point within the mixer at specific encoder positions. The shear rate was calculated every 40° for one complete rotation of the paddles. Because data was not able to be measured for the y velocity, computer simulation results for the y velocity from Ashoken (2008) were used.

Figure 40 shows the calculated values for the shear rate at point 11 for corn syrup. Point 11 is located at a point between the two sides of the twin screw barrel. The shear rate peaks as both paddles approach the point which happens around 120°. Because y velocity data was only available in 40° increments, the plot has wide spaces between data points and each calculation is a different relative paddle position. The only repeat in the paddle orientation is at 0° and 360°.

Figure 41 shows the shear rate calculated for point 27. Point 27 is located on the outside of the left hand barrel where only the left paddle passes it. Point 27 experiences less shear than point 11. Point 11 is very close to the intermeshing region between the

two halves of the barrel and experiences effects from both paddles. Table 3 shows all the shear rates calculated.

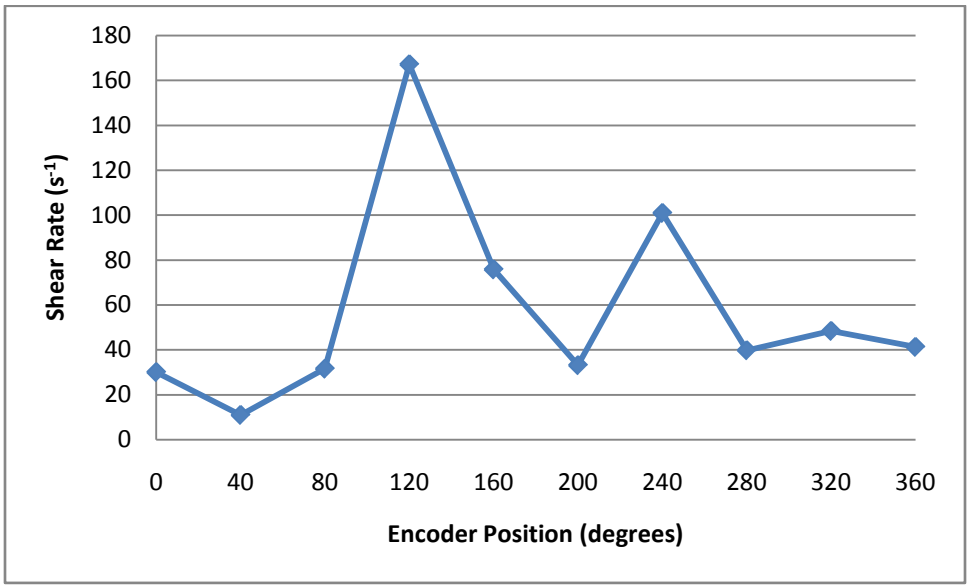

Figure 40 Shear rate for point 11 (corn syrup)

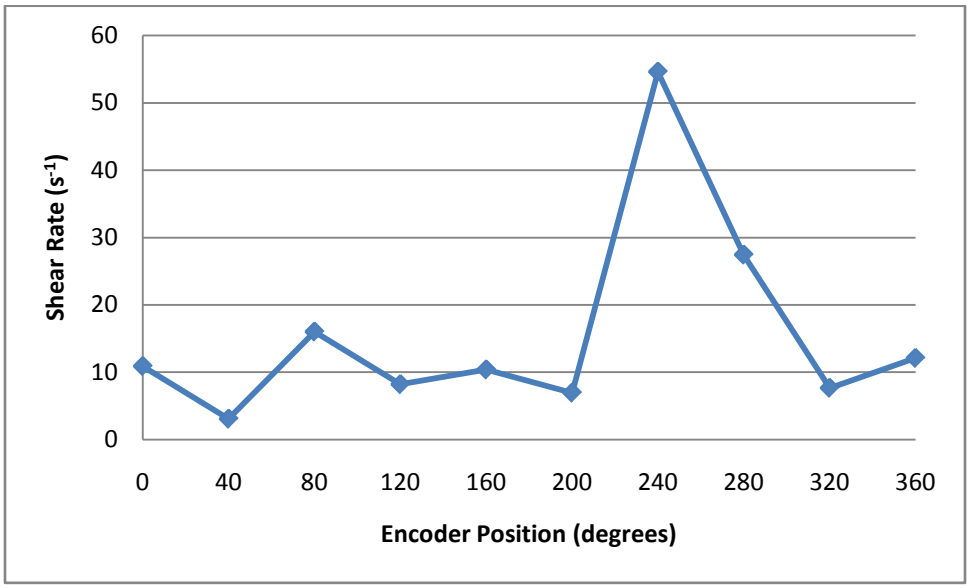

Figure 41 Shear rate for point 27 (corn syrup)

Table 7 Calculated Shear Rates (corn syrup)

Location	0° rotation	40° rotation	80° rotation	120° rotation	160° rotation	200° rotation	240° rotation	280° rotation	320° rotation	360° rotation
1	53.259	33.84	42.702	32.97	52.601	17.422	12.158	79.568	24.852	127.126
2	-	17.997	41.698	37.358	-	-	42.966	92.202	111.078	-
3	55.794	10.739	85.605	27.586	-	19.148	33.389	22.103	22.943	32.003
4	-	13.195	25.952	25.872	-	68.354	31.429	55.889	23.756	-
5	-	3.941	14.94	-	-	-	51.863	1.204	-	-
6	36.824	10.575	18.19	57.103	-	19.566	14.897	46.291	49.289	208.944
7	118.015	32.729	42.848	-	-	20.991	52.588	44.122	-	130.751
8	57.614	8.107	20.721	-	59.206	9.102	42.157	10.522	-	13.333
9	202.954	14.176	35.433	164.453	156.83	40.569	35.639	59.426	-	155.618
10	32.094	84.064	226.686	-	35.845	7.248	41.468	-	-	177.482
11	30.081	11.008	31.6	167.124	75.809	33.174	100.946	39.807	48.408	41.293
12	18.725	30.843	35.171	-	-	68.584	66.101	26.826	-	134.608
13	39.432	12.959	11.211	39.907	44.088	10.786	9.318	19.798	49.642	28.465
14	4.417	14.015	15.668	-	68.509	54.957	18.424	34.021	-	120.328
15	68.757	5.257	118.825	-	-	6.464	1.13E-04	39.164	-	18.776
16	30.503	25.57	16.278	-	18.232	14.607	8.744	9.684	27.779	66.75
17	5.531	16.249	12.264	-	84.384	22.262	57.243	-	-	119.25
18	13.345	2.785	-	-	-	4.036	4.90E-05	-	-	33.764
19	179.899	18.218	-	-	22.873	39.561	22.248	-	23.946	137.301
20	12.428	4.947	-	-	17.882	5.556	-	-	-	86.715
21	43.117	28.492	12.428	8.326	18.132	-	21.037	27.085	14.477	50.267
22	-	-	36.473	28.214	11.201	-	18.682	62.417	20.455	-
23	-	-	12.776	49.376	-	-	-	4.90E-05	76.484	-
24	18.117	-	23.441	15.596	13.473	11.103	50.396	39.438	8.993	17.482
25	13.431	-	29.597	13.452	6.47	-	39.044	11.519	9.766	10.298
26	4.44	-	-	64.879	15.838	-	-	43.302	25.094	6.983
27	10.897	3.093	16.02	8.213	10.396	6.959	54.583	27.431	7.671	12.106
28	15.925	-	-	54.747	15.587	8.993	-	39.375	37.493	16.541
29	3.628	3.967	-	4.253	3.581	4.084	-	-	4.736	23.587
30	13.084	14.955	-	13.242	7.79	14.475	16.868	19.292	13.811	13.298
31	50.081	28.934	-	20.024	21.421	14.319	16.672	15.569	37.387	36.395
32	6.765	3.605	-	2.529	6.486	3.675	-	-	50.358	100.612
33	128.884	46.459	-	15.693	27.634	32.734	-	47.743	26.862	44.963
34	10.179	-	-	6.572	7.042	-	-	2.897	3.869	184.846
35	-	-	-	-	-	-	-	-	-	-
36	41.763	294.89	26.56	17.677	44.852	47.085	24.257	29.388	18.436	37.846
37	91.269	-	12.394	13.086	19.805	29.003	-	4.326	11.119	85.151
38	6.49	-	5.631	2.496	5.635	--	-	8.759	1.981	9.88
39	26.478	20.274	6.996	9.394	34.864	7.94	8.478	27.8	7.522	18.465
40	39.598	5.169	12.905	14.904	69.499	-	9.888	13.553	12.119	19.066

E. Quantifying Mixing

In order to make an objective conclusion about the nature of the mixing taking place in the Readco continuous processor, it is necessary to calculate several measures of the mixing. Both distributive and dispersive mixing need to be quantified. The distributive mixing will tell how us well homogenized the mixture is. The measures of mixing that we will look at are the stretch length ratio, the area stretch ratio, the Manas-Zloczower mixing index and a calculation of the mixing efficiency as calculated in Prakash and Kokini (1999).

1. Instantaneous lineal stretch ratio

To calculate the instantaneous lineal stretch ratio, the rate of change of length vector must be found. When written in matrix form it is given by the following equation

$$\frac{d\bar{l}}{dt} = \begin{bmatrix} \frac{dv_x}{dx} & \frac{dv_y}{dx} & \frac{dv_z}{dx} \\ \frac{dv_x}{dy} & \frac{dv_y}{dy} & \frac{dv_z}{dy} \\ \frac{dv_x}{dz} & \frac{dv_y}{dz} & \frac{dv_z}{dz} \end{bmatrix} \begin{bmatrix} l_x \\ l_y \\ l_z \end{bmatrix}$$

This is a measure of how an individual material element in the fluid stretches with time, t. The length vector of the material, $\bar{l}$, is for each material element at a particular time. The instantaneous stretch ratio can also be written by the following equation:

$$\dot{\boldsymbol{y}} = \boldsymbol{A_v y} \qquad \text{Equation 35}$$

where $\dot{y}$ is the derivative vector, y is the length vector of the material element and A_v is the velocity gradient matrix. The solution for this equation is $y = \left[Xe^{\lambda t}X^{-1}\right]y_0$ where

X is the matrix of eigenvectors of the velocity gradient, λ is the instantaneous lineal stretch ratio defined in equation 16, and y_0 is the initial length vector at t=0.

From the measured data, the velocity gradient is found for each measurement point. The velocity gradient is different for each paddle position at that point. It is found by taking each component of velocity and subtracting the same component's velocity measured at a point a small distance away as in the equation:

$$\frac{dv_x}{dx} = \frac{\Delta v_x}{\Delta x} = \frac{v_{x1} - v_{x2}}{x_1 - x_2} \qquad \textbf{Equation 36}$$

Equivalent equations are used to calculate the velocity gradient for velocity in the y and z direction and for a change in distance in the y and z direction. This shows how the velocity changes with direction. Once these values are known you have the velocity gradient. The components of the velocity gradient are shown by:

$$\overline{\overline{\Delta v}} = \begin{vmatrix} \frac{dv_x}{dx} & \frac{dv_y}{dx} & \frac{dv_z}{dx} \\ \frac{dv_x}{dy} & \frac{dv_y}{dy} & \frac{dv_z}{dy} \\ \frac{dv_x}{dz} & \frac{dv_y}{dz} & \frac{dv_z}{dz} \end{vmatrix} \qquad \textbf{Equation 37}$$

The instantaneous lineal stretch ratio was found for each point at 10 different positions of the paddles. Because *y* velocity was not able to be found experimentally, results from computer simulations carried out by Ashoken (2008) were used for the missing velocities. Starting at 0°, the instantaneous lineal stretch ratio was found at 40° increments. Table 3 shows all the calculated values for the stretch ratio for 0° to 360°. The instantaneous lineal stretch ratio varied at each location with paddle position and did not consistently increase with paddle rotation. To follow the trend of the instantaneous lineal stretch ratio more values were calculated at each point for 10 more rotations of the

paddle at the 360° position. When the values are looked at in the 40° increments for one rotation, for many points the values fluctuate between going up and down. At these points material is being stretched at some paddle positions but is pushed back toward its original position at other paddle positions. Points 1, 6, 16, 21 and 34 experience an exponential increase in stretch ratio value after just one complete rotation of the paddles. Figure 42 shows how the values fluctuate before increasing. There are also breaks in the data because at the paddles blocked points throughout their rotation as indicated in Table 4.

Points 2, 11, 13, 15 and 29 start increasing exponentially after the second rotation. Points 7,18, 25, 31, and 33 do not start increasing exponentially within 10 complete rotations. This is shown in Figure 43. At the 360° position, these points are not being effectively stretched. Points 20 and 32 do seem to have an increasing value of the stretch ratio but increasing very slowly.

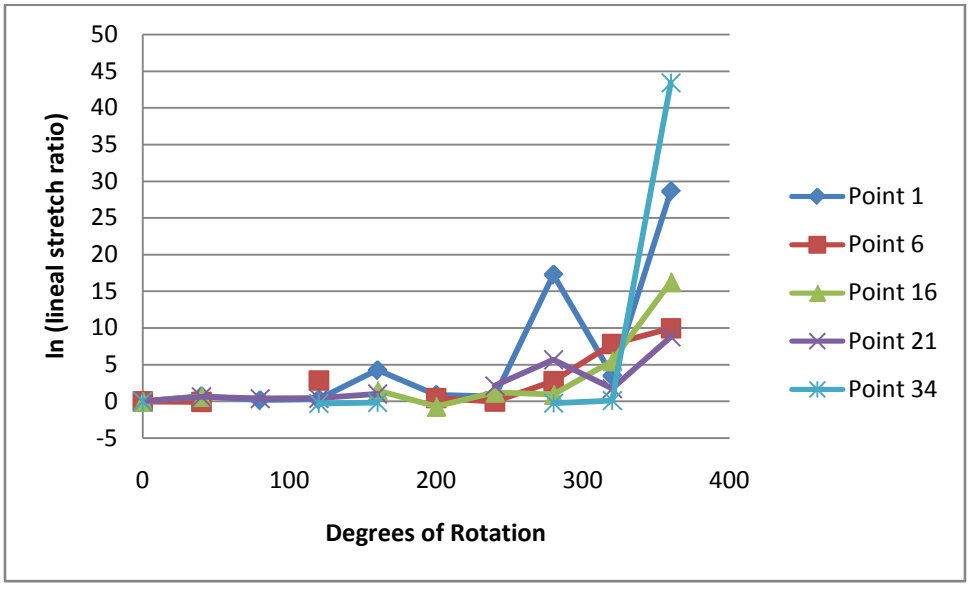

Figure 42 Instantaneous Lineal Stretch for Corn Syrup at 100 rpm

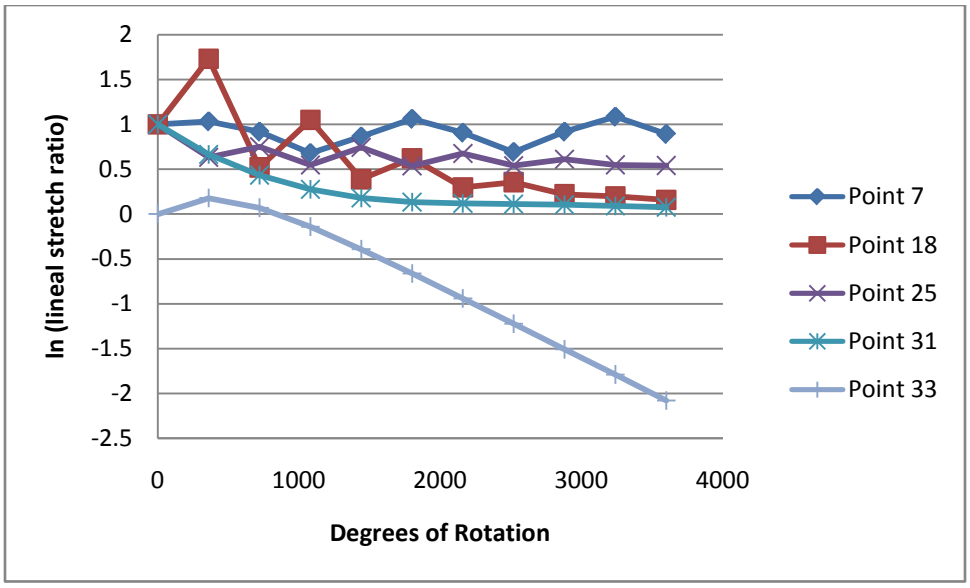

Figure 43 Instantaneous lineal stretch ratio for corn syrup at 100 rpm

Table 8 Instantaneous Lineal Stretch Ratios for corn syrup

Location	40° rotation	80° rotation	120° rotation	160° rotation	200° rotation	240° rotation	280° rotation	320° rotation	360° rotation
1	2.047	1.171	1.33	70.393	2.431	1.954	3.15E+07	33.459	2.65E+12
2	1.243	5.382	24.573	-	-	717.407	5.22E+07	312.852	-
3	0.991	129.127	2.8	-	0.162	61.423	18.021	1.13	30.887
4	1.338	1.951	7.03	-	0.907	205.135	31.528	0.434	-
5	0.973	0.558	-	-	-	7.149	0.903	-	-
6	0.948	-	17.576	-	1.603	1.001	15.713	2.50E+03	2.10E+04
7	0.588	6.242	-	-	1.253	0.458	1.07E+04	-	1.032
8	0.958	3.741	-	0.942	0.873	56.201	1.041	-	1.916
9	0.973	2.707	0.788	4.07E+08	7.673	514.878	1.44E+05	-	4.567
10	5.974	6.40E+05	-	1.26	0.757	7.735	-	-	12.789
11	0.987	2.797	1.16E+04	0.49	1.301	0.653	27.524	44.492	69.411
12	0.401	4.362	-	-	39.274	10.434	10.474	-	2.595
13	1.224		9.289	18.176	0.858	1.677	22.038	167.701	450.614
14	0.773	2.955	-	7.109	201.123	1.033	8.361	-	2.953
15	0.935	12.704	-	-	0.685	-	9.341	-	132.528
16	1.942	-	-	4.378	0.499	3.43	2.536	245.581	1.16E+07
17	0.81	-	-	4.28	13.531	26.848	-	-	4.284
18	0.999	-	-	-	1.094	-	-	-	1.73
19	1.033	-	-	0.392	320.32	52.944	-	153.01	8.77E-03
20	0.963	-	-	1.975	0.938	-	-	-	1.364
21	1.853	1.462	1.534	2.738	-	8.397	286.385	5.686	6.38E+03
22	-	6.465	11.446	2.549	-	0.328	20.804	123.753	-
23	-	0.915	40.082	-	-	-	-	0.807	-
24	-	-	1.389	2.406	0.992	193.748	0.656	4.502	19.036
25	-	0.275	2.08	1.605	-	0.092	1.491	1.433	0.633
26	-	-	1.093	3.108	-	-	44.339	10.642	1.985
27	1.008	1.862	1.746	2.365	2.7	120.862	89.874	3.317	5.142
28	-	-	0.836	0.669	1.631	-	7.453	218.193	5.577
29	1.026	-	1.012	0.923	1.149	-	-	1.431	29.806
30	0.817	-	1.27	0.811	1.791	2.098	2.314	6.382	3.262
31	1.908	-	2.565	3.38	2.511	1.927	1.331	0.713	0.665
32	0.981	-	0.961	0.921	1.041	-	-	0.28	1.198
33	1.946	-	2.333	4.297	22.468	-	5.233	403.483	1.194
34	-	-	0.744	0.834	-	-	0.781	1.093	7.01E+18
35	-	-	-	-	-	-	-	-	-
36	425.661	0.74	1.7	2.667	5.835	2.92	1.069	0.725	11.403
37	-	-	1.984	5.274	2.814	-	0.886	3.509	0.205
38	-	1.086	1.007	0.759	-	-	1.162	1.138	0.532
39	1.419	0.754	0.913	1.864	1.829	1.268	3.651	0.444	0.54
40	1.023	0.542	0.744	5.54E+03	-	0.445	7.502	1.406	2.241

2. Area Stretch

Area stretch is a measure of how much a surface element is stretched during mixing. It is given by the equation

$$a = w \times l \qquad \textbf{Equation 38}$$

Where a is the area of the surface element, l is its length and w is its width. This equation becomes

$$\frac{d\bar{a}}{dt} = -\left(\nabla \bar{v}\right)^T \cdot \bar{a} \qquad \textbf{Equation 39}$$

When Equation 39 is solved the instantaneous area stretch ratio is found. The area stretch was found for the 40 points where measurements were taken. Again velocity data from Ashoken (2008) was used for the *y* velocity. It was calculated at 9 different paddle positions in 40° increments. The values fluctuate for many of the positions but most ultimately increase. None of the points have values that start increasing exponentially during the first rotation. Some of the points have values that do increase exponentially by the end of the 10 revolutions calculated. Points 2, 8, 11, 13, 14, 16, 18, 19, 22, 32, 33, 34, 37, and 38 all have values that start increasing exponentially, although not all of the points reach the same ultimate values in the range that calculations were performed. Figure 44 shows how these points' values behave in the range examined. Figure 45 shows how other measurement points' values of the area stretch behave over the same time. These points have a much more gradual increase in the value of the area stretch.

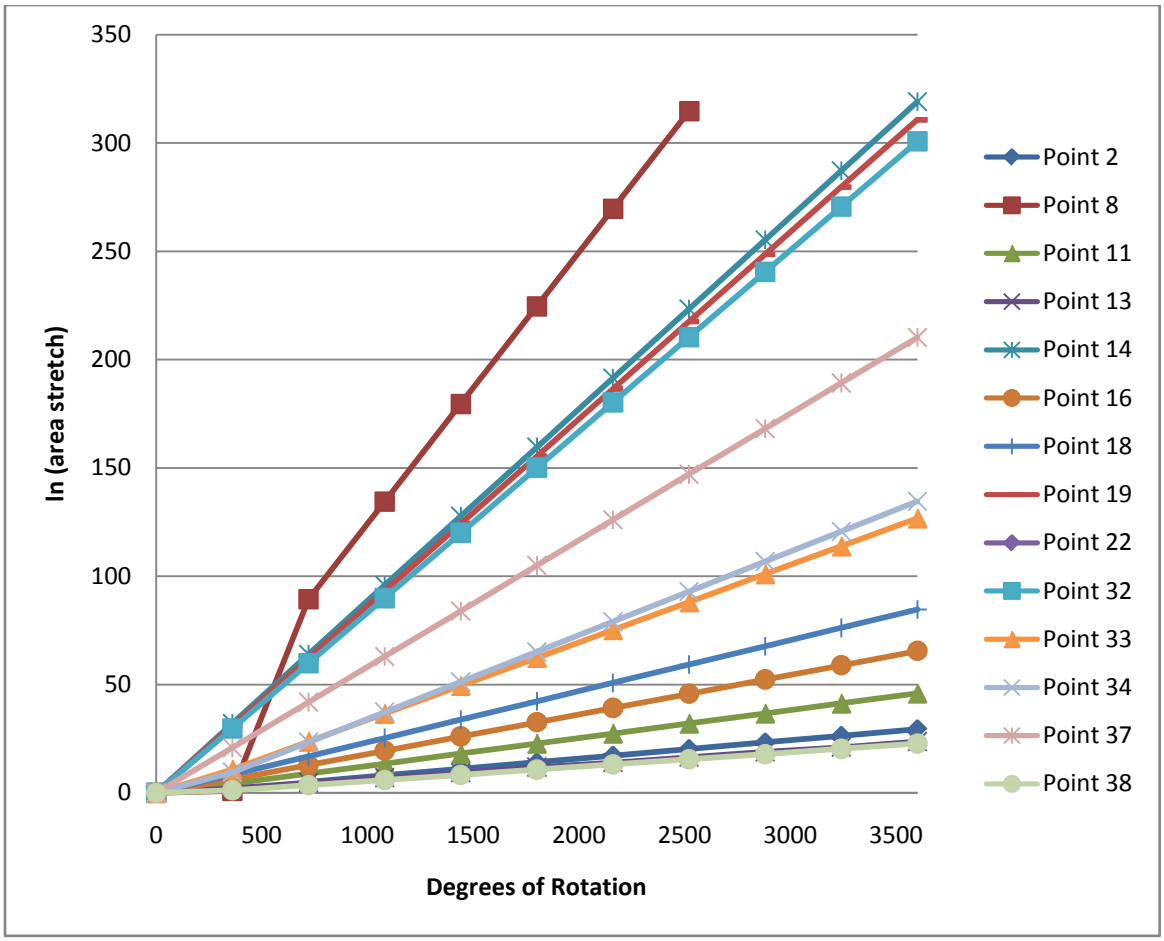

Figure 44 Area Stretch Ratio

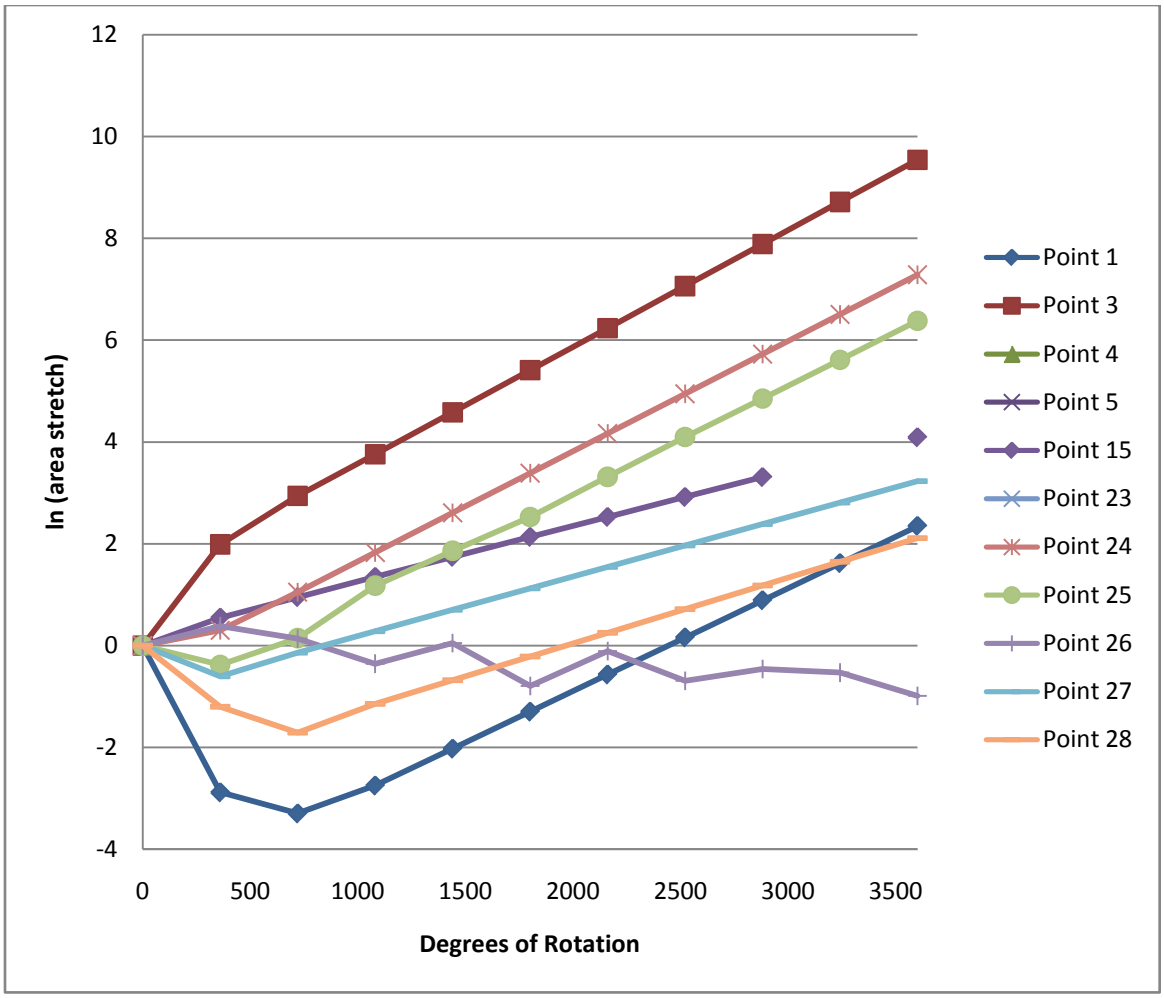

Figure 45 Area Stretch Ratio

Table 9 Area Stretch Ratio for 0° to 360° (corn syrup)

Location	40° rotation	80° rotation	120° rotation	160° rotation	200° rotation	240° rotation	280° rotation	320° rotation	360° rotation
1	0.648	1.142	0.292	0.485	2.084	1.284	1.297	1.558	0.056
2	0.904	1.35	0.118	-	-	6.793	0.83	2.24E+11	-
3	1.076	0.758	2.372	-	7.775	0.809	3.534	16.477	7.304
4	0.783	1.618	1.063	-	269.789	0.806	16.921	4.365	-
5	1.018	0.709	-	-	-	1.799	1.001	-	-
6	1.09	1.687	1.233	-	-	9.917	642.711	2.061	-
7	2.384	0.122	-	-	2.893	1.98E+03	0.857	-	4.15E+16
8	1.066	1.663	-	819.501	1.128	1.038	2.889	-	2.45
9	1.02	0.661	3.50E+05	24.445	3.348	0.604	1.375	-	1.75E+19
10	1.208	13.353	-	40.932	1.83	3.115	-	-	3.98E+22
11	1.028	1.917	1.872	6.36	1.928	2.08E+03	36.901	0.58	68.466
12	2.557	0.566	-	-	5.72	2.589	11.457	-	1.45E+16
13	0.793	0.738	1.423	1.247	1.019	1.046	1.41	0.46	8.173
14	1.362	0.851	-	4.405	1.63	16.723	0.3	-	8.04E+13
15	1.079	6.746	-	-	1.913	-	17.613	-	1.729
16	0.613	0.603	-	1.653	3.516	0.764	2.199	0.508	522.389
17	1.298	1.072	-	9.35	0.619	0.536	-	-	4.13E+14
18	1.006	-	-	-	1.239	-	-	-	4.27E+03
19	1.164	-	-	3.015	0.748	0.059	-	1.725	3.03E+13
20	1.047	-	-	2.953	1.503	-	-	-	7.92E+10
21	0.571	0.789	0.646	1.329	-	1.953	1.072	2.603	3.964
22	-	0.518	0.476	0.874	-	5.809	2.26E+05	0.472	-
23	-	0.817	1.046	-	-	-	-	4.60E+05	-
24	-	0.467	0.653	0.854	3.614	0.442	86.845	0.796	1.353
25	-	3.117	0.338	1.271	-	46.31	2.153	0.214	0.687
26	-	-	35.153	1.722	-	-	5.354	5.89	1.463
27	0.991	0.428	0.832	0.726	0.619	0.622	0.108	0.61	0.545
28	-	-	136.383	5.275	0.752	-	0.516	4.342	0.302
29	0.969	-	0.991	1.209	0.819	-	-	0.917	3.346
30	1.316	-	2.09	0.969	2.304	8.652	15.786	2.555	2.957
31	0.587	-	0.829	0.801	0.673	12.244	9.075	2.744	1.534
32	1.025	-	0.992	1.624	1.184	-	-	0.899	7.47E+12
33	0.863	-	0.633	0.882	1.199	-	1.75E+04	1.019	4.86E+04
34	-	-	0.99	1.681	-	-	1.359	0.794	1.34E+04
35	-	-	-	-	-	-	-	-	-
36	0.328	1.659	0.631	8.435	9.054	21.772	3.144	3.499	1.091
37	-	1.793	0.806	1.946	3.972	-	1.166	4.279	1.07E+09
38	-	0.93	1.056	1.53	-	-	1.239	1.221	3.421
39	0.754	0.838	1.177	3.323	0.94	1.297	2.714	1.374	4.278
40	0.954	1.447	2.629	3.93	-	4.889	2.496	10.032	0.689

Table 10 Area Stretch Ratio for 720° to 3600° (corn syrup)

Location	720° rotation	1080° rotation	1440° rotation	1800° rotation	2160° rotation	2520° rotation	2880° rotation	3240° rotation	3600° rotation
1	0.037	0.064	0.132	0.273	0.566	1.173	2.431	5.04	10.449
2	142.754	3.02E+03	6.37E+04	1.35E+06	2.84E+07	6.00E+08	1.27E+10	2.68E+11	5.65E+12
3	18.913	42.872	97.783	223.391	510.312	1.17E+03	2.66E+03	6.08E+03	1.39E+04
4	-	-	-	-	-	-	-	-	-
5	-	-	-	-	-	-	-	-	-
6	2.37E+53	1.51E+80	9.62E+106	6.14E+133	-	-	-	-	-
7	3.46E+33	2.89E+50	2.42E+67	2.02E+84	1.69E+101	1.41E+118	1.18E+135	9.82E+151	-
8	6.37E+38	2.32E+58	8.44E+77	3.07E+97	1.12E+117	4.07E+136	-	-	-
9	2.45E+45	1.50E+68	9.24E+90	5.68E+113	3.49E+136	-	-	-	-
10	2.45E+45	1.50E+68	9.24E+90	5.68E+113	3.49E+136	-	-	-	-
11	7.04E+03	7.25E+05	7.46E+07	7.67E+09	7.89E+11	8.12E+13	8.36E+15	8.60E+17	8.85E+19
12	2.26E+32	3.52E+48	5.48E+64	8.53E+80	1.33E+97	2.07E+113	3.22E+129	5.01E+145	-
13	113.208	1.08E+03	1.04E+04	1.38E+05	1.13E+06	1.41E+07	1.55E+08	1.30E+09	1.82E+10
14	5.71E+27	4.05E+41	2.88E+55	2.04E+69	1.45E+83	1.03E+97	7.31E+110	5.19E+124	3.69E+138
15	2.588	3.849	5.708	8.454	12.512	18.511	27.38	40.493	59.882
16	3.75E+05	2.69E+08	1.93E+11	1.38E+14	9.90E+16	7.10E+19	5.09E+22	3.65E+25	2.62E+28
17	1.84E+29	8.16E+43	3.63E+58	1.61E+73	7.17E+87	3.19E+102	1.42E+117	6.30E+131	2.80E+146
18	2.03E+07	9.68E+10	4.61E+14	2.19E+18	1.04E+22	4.97E+25	2.36E+29	1.13E+33	5.36E+36
19	9.47E+26	2.96E+40	9.27E+53	2.90E+67	9.06E+80	2.84E+94	8.87E+107	2.77E+121	8.67E+134
20	8.38E+21	8.87E+32	9.39E+43	9.93E+54	1.05E+66	1.11E+77	1.18E+88	1.25E+99	1.32E+110
21	20.856	109.818	578.277	3.05E+03	1.60E+04	8.44E+04	4.45E+05	2.34E+06	1.23E+07
22	-	-	-	-	-	-	-	-	-
23	-	-	-	-	-	-	-	-	-
24	2.853	6.219	13.556	29.545	64.394	140.348	305.892	666.698	1.45E+03
25	1.159	3.248	6.449	12.532	27.57	60.249	128.207	273.995	588.947
26	1.145	0.7	1.052	0.453	0.896	0.501	0.631	0.588	0.373
27	0.866	1.324	2.016	3.074	4.686	7.144	10.891	16.603	25.312
28	0.181	0.319	0.507	0.807	1.285	2.047	3.261	5.195	8.275
29	8.306	20.857	52.527	132.363	333.576	840.688	2.12E+03	5.34E+03	1.35E+04
30	5.381	9.183	15.503	26.123	44.001	74.11	124.82	210.228	354.077
31	2.558	4.939	11.091	27.656	73.029	198.26	544.904	1.51E+03	4.17E+03
32	9.00E+25	1.08E+39	1.30E+52	1.57E+65	1.89E+78	2.28E+91	2.74E+104	3.30E+117	3.97E+130
33	1.90E+10	7.46E+15	2.92E+21	1.15E+27	4.49E+32	1.76E+38	6.90E+43	2.70E+49	1.06E+55
34	1.43E+10	1.53E+16	1.64E+22	1.76E+28	1.89E+34	2.02E+40	2.17E+46	2.33E+52	2.49E+58
35	-	-	-	-	-	-	-	-	-
36	2.359	5.567	13.103	30.84	72.591	170.863	402.172	946.623	2.23E+03
37	1.47E+18	2.02E+27	2.78E+36	3.82E+45	5.24E+54	7.20E+63	9.90E+72	1.36E+82	1.87E+91
38	32.265	359.337	3.97E+03	4.37E+04	4.81E+05	5.30E+06	5.84E+07	6.43E+08	7.08E+09
39	38.594	324.561	2.69E+03	2.23E+04	1.85E+05	1.54E+06	1.28E+07	1.07E+08	8.86E+08
40	3.519	39.953	452.831	5.13E+03	5.81E+04	6.57E+05	7.44E+06	8.43E+07	9.54E+08

3. Manas-Zloczower Mixing Index

The Manas-Zloczower mixing index (λ_{MZ}) is used to describe dispersive mixing. Its value ranges from 0 to 1. A value of 0 means there is pure rotational flow and a value of 1 means there is pure elongational flow. A value of 0.5 would show simple shear flow. The parameter is not frame invariant (Wang and Manas-Zloczower, 2001) and needs to be considered along with the shear stress when determining dispersive mixing. The mixing index is defined by the equation

$$\lambda_{MZ} = \frac{|D|}{|D|+|\Omega|} \qquad \textbf{Equation 40}$$

In Equation 40, D is the stretching rate and Ω is the vorticity. The Manas-Zloczower mixing index was calculated for each of the measured points at every 40° rotation for corn syrup. The values calculated were predominately over 0.5. Only 10 points fell below this value. The greatest number of points fell between 0.6 to 0.7 followed by 0.7 to 0.8. This indicates that the mixing taking place is mostly from a mix of shear and elongational flow. Figure 46 shows the number of points that have Manas-Zloczower parameter numbers within each range of values.

The number of points measured at each range of shear rate values is shown in Figure 47. Over half of the points have a shear rate of less than $30s^{-1}$. The relatively low shear rates would not be very effective for dispersive mixing. So in many sections of the mixer little dispersive mixing would be taking place. In the areas between the paddle tip and barrel wall higher shear is achieved. It is in these areas where particles would be broken apart.

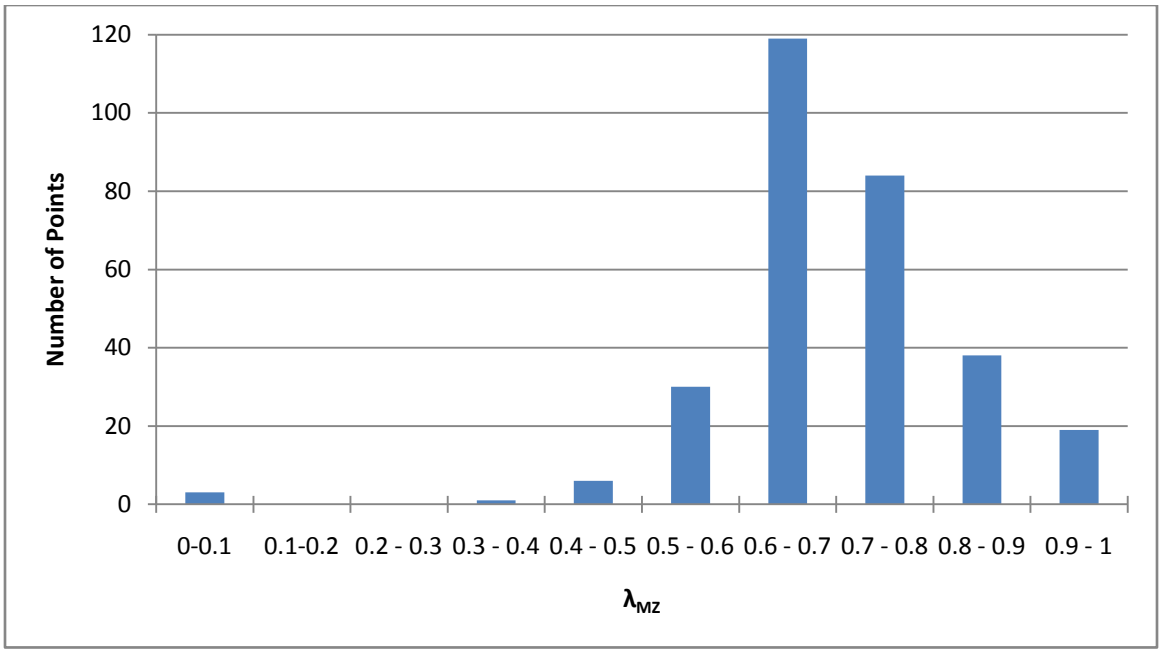

Figure 46 Histogram of Manas-Zloczower parameter values

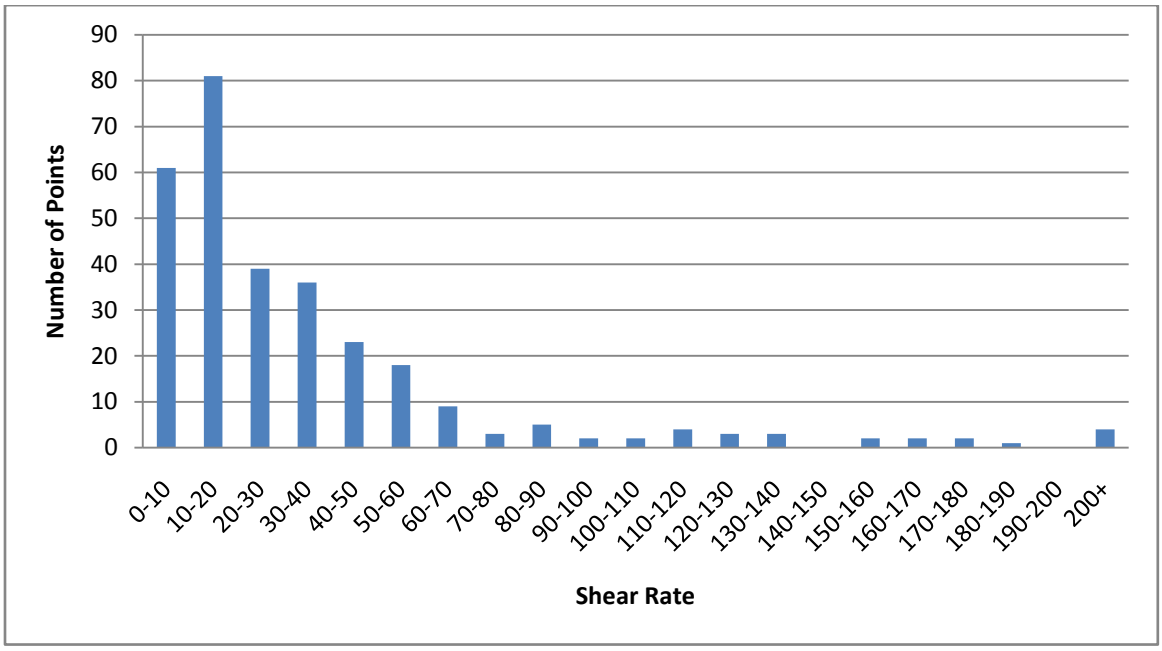

Figure 47 Histogram of Shear Rate Values for measured points

4. Mixing Efficiency

For a process to be good at mixing, it must adequately break up and distribute the different materials of the mixture and form a homogenous mix. A good process does not

necessarily continually cause the break up and separation of particles. Sometimes it may cause unmixing or reagglomeration of particles. The overall result of the process however, must be a separation of particles.

Efficiency of mixing can calculated from Equation 9 based on a number of factors, but here the efficiency is calculated by using the stretch ratio in the method laid out previously. The efficiency was calculated for each of the 40 measurement points at 10 encoder positions 40° apart. The results varied based on the point's location in the paddle rotation. Figure 48 shows the length stretch efficiency calculated for point 1. The efficiency changes throughout the rotation of the paddle. Table 7 shows all the calculated efficiency values.

Figure 48 Efficiency calculated for point 1

Table 11 Calculated Length Efficiency Values

Location	0° rotation	40° rotation	80° rotation	120° rotation	160° rotation	200° rotation	240° rotation	280° rotation	320° rotation	360° rotation
1	0.617	0.641	0.653	0.481	0.556	0.342	0.218	0.96	0.694	0.752
2	-	0.424	0.558	0.854	-	-	0.775	0.822	0.202	-
3	-	-	-	-	-	-	-	-	-	-
4	-	0.631	0.462	0.801	-	0.165	0.82	0.265	-0.28	-
5	-	*-0.248*	*-0.055*	-	-	-	*0.211*	*-0.547*	-	-
6	0.308	-0.117	0.09	0.41	-	0.184	0.05	0.29	0.586	0.164
7	-0.738	0.246	0.622	-	-	0.141	0.017	0.913	-	1.78E-03
8	-0.433	-0.122	0.134	-	-0.131	-0.094	0.493	-0.056	-	0.344
9	-0.556	-0.073	0.356	0.064	0.968	-0.061	0.871	0.855	-	0.079
10	-0.533	0.56	0.93	-	0.089	-0.052	0.247	-	-	0.069
11	-0.206	-0.038	-0.045	0.527	-0.55	0.396	0.047	0.081	0.36	0.67
12	-0.145	-0.84	0.788	-	-	0.345	0.191	0.674	-	0.048
13	-0.387	0.435	1.06	0.556	0.478	-0.129	0.367	0.474	0.352	0.864
14	-0.033	-0.383	1.45E-03	-	0.48	0.518	0.093	-0.096	-	0.031
15	-0.504	-0.356	-0.0012	-	-	-0.217	-0.315	0.125	-	0.879
16	0.078	0.781	0.782	-	0.521	-0.219	0.618	0.567	0.715	0.844
17	0.381	-0.178	-0.152	-	-0.00015	0.87	0.922	-	-	0.045
18	-0.564	0.018	-	-	-	0.336	-0.252	-	-	-0.03
19	0.262	0.08	-	-	-0.044	0.891	0.885	-	0.777	-0.076
20	-0.562	-0.194	-	-	0.375	0.125	-	-	-	9.65E-03
21	0.785	0.588	0.375	0.409	0.187	-	0.427	0.89	0.346	0.549
22	-	-	0.822	0.857	0.5	-	0.186	0.174	0.879	-
23	-	-	-	-	-	-	-	-	-	-
24	0.814	-	0.642	0.216	0.28	0.24	0.475	0.053	0.673	0.613
25	0.19	-	-0.497	0.42	0.619	-	0.208	0.147	-0.039	0.352
26	0.128	-	-	-0.00365	0.482	-	-	0.319	0.196	0.513
27	-0.00015	0.069	0.406	0.779	0.675	0.926	0.315	0.69	0.723	0.219
28	0.718	-	-	0.054	0.162	-0.08	-	-0.203	0.653	0.571
29	-0.413	0.164	-	0.03	-0.035	0.016	-	-	0.283	0.561
30	-0.392	-0.223	-	0.642	6.51E-03	0.448	0.546	0.367	0.588	0.507
31	-0.172	0.603	-	0.378	0.213	-0.0061	0.258	0.122	0.087	-0.333
32	-0.295	-0.133	-	-0.24	0.351	0.38	-	--	0.048	0.016
33	0.401	0.762	-	0.805	0.105	0.606	-	0.137	0.824	-0.0013
34	-0.61	-	-	-0.622	0.377	-	-	0.163	-0.201	0.786
35	-	-	-	-	-	-	-	-	-	-
36	0.669	0.589	-0.362	0.288	-0.037	0.109	0.256	0.035	9.22E-03	0.53
37	-0.737	-	-0.214	0.653	0.693	0.146	-	0.039	0.707	-0.03
38	-0.623	-	0.971	0.163	0.095	-	-	0.122	0.535	0.307
39	0.495	0.449	-0.545	0.185	-0.2	0.465	0.549	-0.045	0.093	-0.165
40	0.505	0.063	-0.185	0.123	0.98	-	-0.159	0.63	0.449	-0.473

V. Conclusions

This work showed some differences in velocity among the different fluids tested. CMC and Carbopol had more similar velocity profiles than that of corn syrup. CMC and Carbopol generally had faster velocities than corn syrup. The differences among them though were not large, generally less than 0.1 m/s. This is due to the shear thinning nature of both CMC and Carbopol. Because their viscosities decrease with shear, they are easier to move through the mixer therefore they tend to have higher velocities.

Comparisons among the mixing quantifiers for the different fluids were not possible because of the lack of *y* velocity data. The corn syrup data did show some differences in how the location within the barrel affects the mixing. Points in the intermeshing region experience more mixing than those on the outer edges of the barrel. Based on their viscosity measurements, CMC and Carbopol should be better mixed in the mixer with the paddle configuration used. Their lower viscosities would allow for more stretching and folding and thus better mixing.

For the calculations performed with the corn syrup data, the results show that there is little stretching and mixing taking place in the outside sections of the barrel. These are the areas where the flow is not broken by the paddle in the other half of the barrel. The fluid is able to move through this section of paddles in a continuous flow. The intermeshing region between the set of paddles experienced the most mixing. This is due to the paddle configuration used to do this work. Because the set of nine paddles were all aligned the flow in this experiment, the flow was not broken and interrupted enough for good mixing of the fluid to be achieved. Other configurations of the equipment would produce better mixing results.

The velocity results do allow for comparison with computer simulation performed on the same system. The results showed there was good agreement between experimental and simulation results. The difference in values was 12.3% for the x velocity and 2.1% for the z velocity. Based on couette flow measurements an error around 9% could be expected. The z velocity results probably agree better because the flow in the z direction is more like plug flow with not as much variation as in the x direction. This provides validation, a link often missing between simulations and real mixing systems.

VI. References

Adrian, R.J. (1991). Particle-imaging techniques for experimental fluid mechanics. Annu. Rev. Fluid Mech., 23, 261-304.

Alemaskin, K., Manas-Zloczower, I., and Kaufman, M. (2004). Index for simultaneous dispersive and distributive mixing characterization in processing equipment. International Polymer Processing, XIX, 327-334.

Almond, N. (1989). Biscuits, cookies and crackers: the biscuit making process (Vol. 2). New York: Elsevier Applied Science.

Arratia, P.E., Kukura, J., Lacombe, J. and Muzzio, F.J. (2006). Mixing of shear-thinning fluids with yield stressin stirred tanks. AIChE Journal, 52(7), 2310-2322.

Ashokan, B.K. (2008). Developing Methods for Design and Analysis of Continuous Mixers Through 3D Numerical Simulation of Flow and Mixing. PhD Dissertation. Rutgers, The State University of New Jersey, New Brunswick, NJ.

Bakalis, S. (1999). Measurement of Velocity Distributions in the Screw Channels of a Co-rotating Twin-screw extruder. PhD Dissertation. Rutgers, the State University of New Jersey.

Bakalis, Serafim and Mukund V. Karwe (2002). Velocity distributions and volume flow rates in the nip and translational regions of a co-rotating, self-wiping, twin-screw extruder. Journal of Food Engineering. 51 273-282.

Bicen, A. F. (1982). Refraction correction for LDA measurements in flows with curved optical boundaries. TSI Quarterly, VIII, 10-12.

Bird, R.B, Armstrong, R.C. and O. Hassager (1987). Dynamics of Polymeric Liquids: Vol. 1 Fluid Mechanics. New York: John Wiley & Sons, Inc.

Bird, R.B, Stewart, W.E. and E.N. Lightfoot (2002). Transport Phenomena. John Wiley & Sons, Inc.

Brodkey, R.S. (1985). Fundamentals of turbulent mixing and kinetics. In Ulbrecht, J.J. and Patterson, G.K. (Eds.), Mixing of Liquids by Mechanical Agitation (pp. 29-58). New York,: Gordon and Breach Science Publishers.

Chen, K., Hajduk, J.C., and J.W. Johnson. (1988). Laser-Doppler Anemometry in a Baffled Mixing Tank.Chemical Engineering Communication, 72, 141-157.21

Connelly, R.K. and Kokini, J.L. (2004). The effect of shear thinning and differential viscoelasticity on mixing in a model 2D mixer as determined using FEM with particle tracking. Journal of Non-Newtonian Fluid Mechanics, 123, 1-17.

Connelly, R.K. and Kokini, J.L. (2007). Examination of the mixing ability of single and twin screw mixers using 2D finite elemnt method simulation with particle tracking. Journal of Food Engineering, 79, 956-969.

Doraiswamy, D., Grenville, R.K. and A.W. Etchells III (1994). Two-score years of the Metzner-Otto correlation. Ind Eng Chem Res, 33(10), 2253-2258.

Durst, F, Melling A. and J.H. Whitelaw (1981). Principles and Practice of Laser-Doppler Anemometry. Academic Press.

Fischer, M., Jovanovic, J., and F. Durst. (2001). Reynolds Number Effects in teh Near-Wall Region of Turbulent Channel Flows. Physics of Fluids, 13, 1755-1767.

Herucles Incorporated. (2000). Aqualon CMC brochure. Retrieved March 7, 2001 from http://www.herc.com/aqualon/product_data/aq_bro_cmc_intro.htm

Lawler, J.V, Muller, S.J, Brown, R.A, and R.C. Armstrong. (1986). Laser Doppler Velocimetry Measurements of Velocity Fields and Transitions in Viscoelastic Fluids. Journal of Non-Newtonian Fluid Mechanics.20, 51-92.

Li, T. and Manas-Zloczower, I. (1995). Evaluation of distributive mixing efficiency in mixing equipment. Chem. Eng. Comm., 139, 223-231.

Matz, S.A. (1992). Bakery Technology and Engineering (3rd ed.). New York: Van Nostrand Reinhold.

Mavros, P., Naude, I., Xuereb, C., and J. Bertrand. (1997). Laser Dopppler Velocimetry in Agitated Vessels: Effect of Continuous Liquid Stream on Flow Patterns. Trans IChemE, 75A, 763-776.

Metzner, A.B., Feehs, R.H., Ramos, H.L., Otto, R.E., and Tuthill, J.D. (1961). Agitation of viscous Newtonian and non-Newtonain fluids. AIChE Journal, 7(1), 3-9.

Metzner, A.B. and Otto, R.E. (1957). Agitation of non-Newtonian fluids. AIChE Journal, 3(1), 3-10.

Metzner, A.B. and Taylor, J.S. (1960). Flow Patterns in Agitated Vessels. AIChE Journal, 6(1), 109-114.

Norwood, K.W. and Metzner, A.B. (1960). Flow patterns and mixing rates in agitated vessels. AIChE Journal, 6(3), 432-437.

Oldshue, J.Y. (1983). Fluid Mixing Technology. New York: McGraw-Hill Publications.

Ottino, J.M. (1989). The Kinematics of Mixing: Stretching, Chaos, and Transport. Cambridge University Press, New York.

Prakash, S. (1996). Characterization of Shear Rate Distributionin a Model Mixer Using Laser-Doppler Anemometry. PhD Thesis. Rutgers, the State University of New Jersey.

Prakash, Subbalakshmi and Jozef L. Kokini (1999). Determination of Mixing Efficiency in a Model Food Mixer. Advances in Polymer Technology, vol 18. no. 3, 209-224.

Ranz, W.E. (1985). Fluid mechanical mixing - lamellar description. In Ulbrecht, J.J. and Patterson, G.K. (Eds.), Mixing of Liquids by Mechanical Agitation (pp. 1-28). New York,: Gordon and Breach Science Publishers.

Schafer, M., Hofken, M., and F. Durst. (1997). Detailed LDV Measurements for Visualization of the Flow Field within a Stirred-Tank Reactor Equipped with a Rushton Turbine. Trans IChemE, 75, part A, 729-736.

Schmidt, M., Wassner, E., and H. Munstedt. (2000). Setup and Test of a Laser Doppler Velocimeter for Investigations of Flow Behaviour of Polymer Melts. Mechanics of Time-Dependent Materials, 3, 371-393.

Tadmor, Z. and Gogos, C.G. (2006). Principles of Polymer Processing (2^{nd} ed.). Hoboken, NJ: John Wiley & Sons.

Unger, D.R., Muzzio, F.J., Aunins, J.G. and Singhvi, R. (2000). Computational and experimental investigation of flow and fluid mixing in the roller bottle bioreactor. Biotechnology and Bioengineering, 70(2), 117-130.

Wang, W. and Manas-Zloczower, I. (2001). Temporal distributions: The basis for the development of mixing indexes for scale-up of polymer processing equipment. Polymer Engineering and Science, 41, 1068-1077.